THE JOURNAL OF BIOLOGICAL CHEMISTRY VOL. 290, NO. 41, pp. 24816–24834, October 9, 2015

Hsp31 Is a Stress Response Chaperone That Intervenes in the Protein Misfolding Process*

Received for publication, July 15, 2015, and in revised form, August 17, 2015 Published, JBC Papers in Press, August 25, 2015, DOI 10.1074/jbc.M115.678367

Chai-jui Tsai[‡1,2], **Kiran Aslam**[‡1,3], **Holli M. Drendel**[‡], **Josephat M. Asiago**[‡], **Kourtney M. Goode**[‡], **Lake N. Paul**[§], **Jean-Christophe Rochet**[‡], **and Tony R. Hazbun**[‡4]

From the [‡]*Department of Medicinal Chemistry and Molecular Pharmacology and Purdue University Center for Cancer Research and the* [§]*Bindley Bioscience Center, Purdue University, West Lafayette, Indiana 47907*

Background: Hsp31 is a multifunctional cellular stress response protein.
Results: Hsp31 is a stress-inducible chaperone that has substoichiometric activity on a wide spectrum of substrates, including prions and the non-physiological client, α-synuclein.
Conclusion: Hsp31 protects cells from α-synuclein-mediated toxicity via chaperone activity and independently from enzymatic activity and autophagy.
Significance: This is the first characterization of the early acting and wide ranging chaperone activity of Hsp31.

The *Saccharomyces cerevisiae* heat shock protein Hsp31 is a stress-inducible homodimeric protein that is involved in diauxic shift reprogramming and has glyoxalase activity. We show that substoichiometric concentrations of Hsp31 can abrogate aggregation of a broad array of substrates *in vitro*. Hsp31 also modulates the aggregation of α-synuclein (αSyn), a target of the chaperone activity of human DJ-1, an Hsp31 homolog. We demonstrate that Hsp31 is able to suppress the *in vitro* fibrillization or aggregation of αSyn, citrate synthase and insulin. Chaperone activity was also observed *in vivo* because constitutive overexpression of Hsp31 reduced the incidence of αSyn cytoplasmic foci, and yeast cells were rescued from αSyn-generated proteotoxicity upon Hsp31 overexpression. Moreover, we showed that Hsp31 protein levels are increased by H_2O_2, in the diauxic phase of normal growth conditions, and in cells under αSyn-mediated proteotoxic stress. We show that Hsp31 chaperone activity and not the methylglyoxalase activity or the autophagy pathway drives the protective effects. We also demonstrate reduced aggregation of the Sup35 prion domain, PrD-Sup35, as visualized by fluorescent protein fusions. In addition, Hsp31 acts on its substrates prior to the formation of large aggregates because Hsp31 does not mutually localize with prion aggregates, and it prevents the formation of detectable *in vitro* αSyn fibrils. These studies establish that the protective role of Hsp31 against cellular stress is achieved by chaperone activity that intervenes early in the protein misfolding process and is effective on a wide spectrum of substrate proteins, including αSyn and prion proteins.

Heat shock proteins (HSPs)[5] protect living cells against environmental stress and promote cell survival. This function is evolutionarily conserved throughout different organisms. HSPs interact with misfolded proteins and process them using several mechanisms, including chaperone functions to prevent misfolded protein aggregation, unraveling protein aggregates, or carrying out protease functions to eliminate irreversibly damaged proteins. The effect of HSPs in maintaining cellular homeostasis throughout the protein folding process is essential to preventing diseases associated with protein misfolding and aggregation, such as Alzheimer disease, Parkinson disease (PD), and Huntington disease. HSPs involved in counteracting these protein inclusions are currently under intensive study (1).

Among the neurodegenerative diseases, PD is the second most common neurodegenerative disorder that occurs in elderly individuals 50 years or older, and no cure is currently known (2, 3). High levels of reactive oxygen species (ROS), dysfunctional mitochondria, and the aggregation of αSyn are observed in PD (4–8). *DJ-1*, a gene linked to familial forms of PD, has been found to be involved in oxidative insults, proteasome degradation, and protein folding and is the focus of extensive studies to understand its functions in regulating levels of αSyn aggregation (9–14).

Human DJ-1, yeast Hsp31 (YDR533c), and *Escherichia coli* Hsp31 (*hchA* or *yedU*) are members of the DJ-1/PfpI/ThiJ superfamily (10, 15, 16). Crystal structures of Hsp31 show that it contains a cysteine catalytic triad that is conserved in the DJ-1/PfpI/ThiJ family (17, 18). *E. coli* hchA is a close ortholog with yeast Hsp31, and they share superimposable active sites in each monomer, but their quaternary structures appear to be different (17, 19). This protein family is of biomedical importance due to the role these proteins play in chaperone-like and

* This work was supported, in whole or in part, by National Institutes of Health, National Center for Advancing Translational Sciences, Clinical and Translational Sciences Award UL1TR001108 and National Institutes of Health Grant R01 GM087461 (to the Indiana Clinical and Translational Sciences Institute). This publication also supported by a Showalter Foundation grant (to J-C. R. and T. H.). The authors declare that they have no conflicts of interest with the contents of this article.
[1] Both authors contributed equally to this work.
[2] Supported in part by a Purdue Research Foundation fellowship.
[3] Supported by a Fulbright Foundation fellowship, United States Education Foundation - Pakistan.
[4] To whom correspondence should be addressed: Dept. of Medicinal Chemistry and Molecular Pharmacology, Purdue University, 575 Stadium Mall Dr., West Lafayette, IN 47906. E-mail: thazbun@purdue.edu.

[5] The abbreviations used are: HSP, heat shock protein; αSyn, α-synuclein; PD, Parkinson disease; ROS, reactive oxygen species; MGO, methylglyoxal; SD, synthetic dextrose; CS, citrate synthase; SC, synthetic complete; SDD-AGE, semidenaturing detergent-agarose gel electrophoresis; PrD, prion-forming domain(s); CFP, cyan fluorescence protein; EYFP, enhanced yellow fluorescence protein; DsRed, red fluorescence protein from *Discosoma* sp.; MORF, yeast movable ORF tag.

TABLE 1
Yeast strains

Strain	Genotype	Source/Reference
BY4741	*MATa his3, leu2, met15, ura3, ARL1, GCS1, ARL3, ARF3, YPT6, IMH1, SYS1, GAS1*	Invitrogen
W303-1A	*MATa can1-100 his3-11,15 leu2-3, 112 trp1-1 ura3-1 ade2-1*	R. Rothstein
W303-*hsp31*Δ	*W303-1A hsp31*Δ*μ*:natMX	This study
W303-*HSP31-9myc*	*W303-1A HSP31-9myc*::kanMX	This study
W303–1xαSyn	W303 *GAL*-αSyn-YFP at *URA3* or *TRP1* loci	J-C. Rochet (75, 76)
W303–2xαSyn	*W303 GAL*-αSyn-YFP at *URA3 GAL*-αSyn-CFP at *TRP1* loci	J-C. Rochet

cytoprotective activities (15, 19). Despite the shared structural similarity, this family can be further subcategorized into three classes according to the structural and functional properties of the proteins or into five subclasses by protein sequence alignments (15, 19). The cellular functions of DJ-1 and *E. coli* hchA have been characterized, and their multifunctional roles in mediating oxidative stress, chaperone-like activity, methylglyoxalase activity, and cytoprotection have been described (10, 15, 16, 19). There has been limited characterization of the cellular functions of Hsp31, but several recent studies have demonstrated that it has glyoxylase activity (20), chaperone activity (21), and a role in autophagy (22).

Yeast PD models have been used to study the mechanism of the sporadic and familial forms of PD (23–25). We are extending the utility of these yeast models by investigating the biological activities of yeast Hsp31. Hsp31 appears to be a stress-inducible 26-kDa protein based on several large scale studies indicating that yeast Hsp31 is up-regulated when cells are exposed to environmental stress (26–29). For example, Hsp31 was implicated to be protective against ROS because an *hsp31*Δ strain was more sensitive to oxidative stress (26). HchA has structural similarity to Hsp31 and is established as having chaperone activities, suggesting that Hsp31 could act similarly; however, this has yet to be confirmed. The evidence for a role in stress response, possible chaperone activity, methylglyoxalase activity, and cross-talk with the autophagy pathway led us to investigate these activities of Hsp31 in modulating αSyn cytoplasmic foci formation and prion aggregation. αSyn is not present in yeast and hence is a non-physiological substrate, but it mimics physiologically relevant activity based on its localization and toxicity, and we capitalized on these features. Therefore, we designed a set of biochemical, genetic, and cell biology experiments to demonstrate the role of Hsp31 chaperone activity in protecting cells from αSyn-mediated cytotoxicity. We also demonstrate that Hsp31 has methylglyoxalase activity that converts methylglyoxal (MGO) substrate to D-lactate, but this enzyme activity is not essential for protecting against αSyn-mediated cytotoxicity.

Experimental Procedures

Yeast Cell Growth Conditions

Yeast media were prepared according to Amberg *et al.* (30). Liquid yeast extract/peptone dextrose medium contained Bacto yeast extract (1%; Fisher), Bacto peptone (2%; Fisher), and glucose (2%; Fisher). Synthetic dextrose (SD) minimum liquid medium was made of 0.17% Difco yeast nitrogen base (without amino acids) and 2% glucose and supplemented with necessary amino acids for auxotrophic strains needed at concentrations described previously (30). Solid medium plates were made with the same components of liquid medium plus 2% agar (Fisher). To express galactose-inducible proteins, 2% raffinose (Affymetrix, Cleveland, OH) and 2% galactose (Affymetrix) were used to replace glucose. Fractions of culture were obtained at designated times to monitor the cell fitness and protein levels by A_{600} and immunoblotting, respectively.

All of the yeast strains were grown at 30 °C in 2% glucose minimal medium overnight. Strains were diluted to A_{600} of 0.2 and grown in minimal medium switching the carbon source with 2% raffinose for the overnight period. Cultures were normalized to A_{600} of 0.8, and 5-fold serial dilutions were aliquoted onto the respected appropriate dropout plate containing 2% glucose or galactose. Plates were incubated at 30 °C for 2–3 days.

Yeast Strain Construction

Yeast strains used in this study are listed in Table 1. The *hsp31*Δ and *atg8*Δ deletions were generated in W303-1A or in a strain expressing one or two copies αSyn fused to fluorescent proteins (CFP and YFP) using the primers listed in Table 2. The *nat* (nourseothricin *N*-acetyltransferase) gene flanked by Hsp31 homology regions was obtained by PCR with 70-nucleotide-long forward primer and reverse primer. The primers consisted of 20 nucleotides for amplifying the *nat* gene from pFA6a-natNT2 (Euroscarf) and 50 nucleotides immediately preceding the *HSP31* or *ATG8* start codon or after the stop codon. The amplified product was integrated into W303 αSyn-expressing strains at ChrIV:1502160 to 1501447, as described previously (31). For double knock-out *hsp31*Δ *atg8*Δ strain, the kanMX4 resistance cassette was used to delete Hsp31, and then the natMX4 resistance cassette was used for deletion of *ATG8*.

Hsp31–9myc Tagging

We endogenously tagged *HSP31* with the 9myc epitope using a PCR-based integration (12). The pYM20 plasmid was used as a template, and primers were used to obtain PCR product with *HSP31* genomic flanking followed by transformation into W303 and W303 αSyn-CFP + αSyn-YFP strains. The transformants were selected on media containing hygromycin B (300 mg/liter), and correct integration was verified by PCR using primers spanning the integration junctions and by DNA sequence analysis.

DNA Manipulation

The plasmids used in this study are listed in Table 3. Plasmid BG1805 was linearized with NdeI (New England Biolabs, Ipswich, MA) and cloned into pDONR221 (Invitrogen) with BP Clonase (Invitrogen) with the method provided by the manufacturer. Hsp31 was shuttled into pAG415-*GPD-ccdB*-DsRed

TABLE 2
Primers

Gene/Description	Forward	Reverse
HSP31 deletion	AAGTACTTCCCACTGGCTAATTACACAGATAAAACTCAAACAAA TTTATAATGACATGGAGGCCCAGAATACCC	CTTACATCTATATAGTAGTACAAAGGAAATTCTAATTATC AACCTTTGGCTCACAGTATAGCGACCAGCATTCAC
9myc tag of *HSP31*	TCTGCGCACTCCACTGCCGTAAGATCCATCGACGCTTTAAAAA ACCGTACGCTGCAGGTCGAC	TCCTTACATCTATATAGTAGTACAAAGGAAATTCTAATTAT CAACCTTTGGCTCAATCGATGAATTCGAGCTCG
HSP31	AAACTCGAGATGGCCCCAAAAAAAGTTTTACTCGC	TTTGCTAGCTCAGTTTTTTAAAGCGTCGATGGATCTTAC
ATG8 deletion	AGTTGAGAAAATCATAATAAAATAATTACTAGAGACATGACAT GGAGGCCCAGAATACCC	CGATTTTAGATGTTAACGCTTCATTTCTTTTCATATAAAA GACTACAGTATAGCGACCAGCATTCAC
HSP31 mutation C138D	GTTGATCACGGTCCTGCTATTTTTGATGGG	GTGATCAACAGCTGCGACAACACCACCG
ATG8 deletion diagnostic	GGGAACCATTAAAGGTTGAGGAGG	GTAAACATTCTTATACTGGAACA
HSP31 9myc tag diagnostic	ACAGAGAATTAACGTTACTCATTCC	ATATTTGGATATTGGGGAAACACAT
HSP31 deletion diagnostic	TTCGTGGTCGTCTCGTACTC	GCAGGGCATGCTCATGTAGA

TABLE 3
Plasmids

Plasmids	Type of plasmid	Source/Reference
BG1805 *HSP31-MORF*	Yeast, 2 μ	Gelperin *et al.* (77)
pGEX6P-1 *HSP31*	*E. coli*	This study
pESC-Leu	Yeast, 2 μ	Agilent Technologies
pESC-Leu *myc-HSP31*	Yeast, 2 μ	This study
pNT-hchA His6-hchA	*E. coli*	Sastry *et al.* (78)
pT7 αSyn	*E. coli*	Paleologou *et al.* (33)
pAG415-*GPD-HSP31*-DsRed	Yeast, CEN	This study
pAG415-ccdB-DsRed	Yeast, CEN	Alberti *et al.* (39)
pAG424-*GAL*-PrD-Sup35-EYFP	Yeast, 2 μ	Alberti *et al.* (79)
p2HG-*GPD-HSP104*	Yeast	J-C. Rochet
p2HG-*GPD*	Yeast	J-C. Rochet

(Addgene, Cambridge, MA) (32) from pDONR221 with LR Clonase (Invitrogen) to produce pAG415-*GPD-HSP31*-DsRed. Both *DJ-1* and Hsp31 were cloned into BamHI/XhoI sites of pGEX 6p-1. pESC-Leu *myc-HSP31* was constructed by cloning at the XhoI/NheI sites. The *HSP31* gene was amplified from yeast genomic DNA. The Hsp31 C138D mutant was prepared by PCR amplification using pAG415-*GPD-HSP31*-DsRed as template and the set of primers listed in Table 2. Each successfully mutated insert was sequenced to confirm the mutation.

Antibodies and Immunoblotting

To determine protein expression, yeast cells were collected by centrifuging at 5,000 rpm, and pellets were resuspended in extraction buffer (50 mM Tris-HCl, pH 7.5, 1 mM EDTA, 4 mM $MgCl_2$, 5 mM DTT). Glass beads (Sigma) were added into the mixture, which was vortexed 5 times for 10 s each, plus 1-min intervals on ice. Clear crude protein lysate was obtained by spinning down the cell debris at 1,000 × *g* at 4 °C for 10 min. The SDS-PAGE loading dye (4% SDS, 40% glycerol, 0.02% bromphenol blue, Tris-Cl, pH 6.8) was added to the supernatant, and samples were boiled, followed by SDS-PAGE and immunoblotting with antibodies. Monoclonal anti-Myc and anti-β-actin antibody were purchased from Sigma-Aldrich. Monoclonal anti-αSyn was obtained from BD Biosciences. Antibodies were used to detect expression of Hsp104 (ab69549, Abcam), Hsp70 (SPA-82, Stressgen); DsRed (Sc-33353, Santa Cruz Biotechnology, Inc.), and GFP (anti-GFP, Roche Applied Science).

Protein Purification

BY4741 harboring yeast Hsp31 expression plasmid from the yeast moveable ORF collection (33) (Thermo Fisher Scientific) was used to express and purify the protein (33). We did not see any evidence of co-purifying proteins on SDS-polyacrylamide gels and observed similar high activity from protein purified under high salt conditions, which minimizes contaminant co-purifying proteins. Human *DJ-1* was encoded in pGEX 6p-1 (GE Healthcare), *hchA* was encoded in pNT-hchA, and αSyn was expressed from the pT7 plasmid. The protein expression and purification was described previously (34–36). Briefly, constructs were transformed into BL21 (DE3) cells. The transformants were grown to an A_{600} of 0.4–0.6 in LB medium supplemented with 100 μg/ml ampicillin at 37 °C, and isopropyl β-D-1-thiogalactopyranoside (1 mM final concentration) was added to induce protein expression. After 3 h of induction at 37 °C, cells were harvested by centrifugation at 2,000 × *g* and resuspended in lysis buffer (25 mM KP_i, pH 7.0, 200 mM KCl) containing protease inhibitor mixture set IV (Calbiochem). Crude protein was prepared by sonicating cells and clarifying the lysate by centrifugation at 10,000 × *g* for 10 min. GST-tagged DJ-1 was immobilized by glutathione-agarose resin (Thermo Scientific), and DJ-1 was eluted by cleaving from the GST tag with PreScission Protease (GE Healthcare) (2 units of protease for every 100 μg of tagged DJ-1), leaving a linker amino acid sequence: NPAFLYKVVDVSRHHHGRIFYPY-DVPDYAGLEVLFQ.

Sedimentation velocity ultracentrifugation was performed with two different Hsp31 concentrations (34 and 17 μM) and run at 50,000 rpm in a Beckman Coulter XLA centrifuge (Beckman Coulter, Fullerton, CA). The sedimentation coefficients and apparent molecular weights were calculated from size distribution analyses ($c(s)$) using SEDFIT (37).

His_6-hchA was immobilized by HIS-Select® nickel affinity gel (Sigma-Aldrich) and eluted with elution buffer (Tris-Cl, pH 7.5, 250 μM imidazole). The purity of proteins was determined by SDS-PAGE followed by Coomassie Blue staining, and concentrations were determined by a Micro BCA protein assay kit (Thermo Scientific, Waltham MA). The αSyn protein for *in vitro* fibrillization assays was purified by expressing pT7-7 plasmid containing human αSyn cDNA (provided by R. Jakes and M. Goedert, Medical Research Council, Cambridge, UK) with isopropyl β-D-1-thiogalactopyranoside in BL21 (DE3) for 4 h of incubation at 37 °C. The cells were harvested and resuspended in 10 mM Tris-Cl, pH 8, 1 mM EDTA, 1 mM PMSF at ½0 culture volume. The cell lysate was obtained by one round of freeze-thawing and French press treatment, and protein was partially purified and enriched by two rounds of ammonium sulfate precipitation (30% saturation first and then 50% saturation at 0 °C). The pellets were resuspended and boiled in 10 mM Tris-HCl, pH 7.4, for 5 min. The insoluble protein was removed by centrifugation, and the supernatant was filtered using a 0.22-μm

filter. The filtered fraction of the protein was applied to a DEAE-Sepharose FF column (GE Healthcare) with 10 mM Tris-HCl, pH 7.4, and eluted with 0–500 mM NaCl over 100 min. The fractions containing αSyn were dialyzed against 10 mM NH_4HCO_3 and lyophilized. The protein was ~95% pure based on Coomassie Blue staining with SDS-PAGE.

Chaperone Activity Aggregation Suppression Assays

Thermal Aggregation Assay of Citrate Synthase (CS)—CS aggregation suppression assay was performed according to the procedures described previously (38). Briefly, CS (porcine CS, Sigma), Hsp31, DJ-1, and hchA were buffer-exchanged into 40 mM Hepes-KOH (pH 7.5). Proteins were diluted to concentrations ranging from 0.1 to 0.6 μM in a 500-μl reaction. Samples were loaded into a quartz cuvette and placed into the FluoroMax-3 spectrofluorometer (Horiba, John Yobin) heated to 43 °C. Aggregation of CS, with and without Hsp31, was measured by light scattering with the excitation and emission set to 360 nm and a slit width of 2 nm. BSA fraction V and hchA served as negative and positive controls. Measurements were taken every second for 2,000 s. Data were plotted using GraphPad Prism version 5.0.

Reducing Agent-induced Aggregation of Insulin (38, 39)—Briefly, Hsp31 was buffer-exchanged into PBS (pH 7.2). Insulin was diluted with PBS to 26 μM, and 4 or 8 μM of Hsp31 was used in a 500-μl reaction. Samples were loaded into a quartz cuvette and placed into the FluoroMax-3 spectrofluorometer. Aggregation of insulin induced by 20 mM DTT, with and without Hsp31, was measured by light scattering with the excitation and emission set to 360 nm and a slit width of 1 nm. Measurements were taken every second for 2,000 s. Data were plotted using GraphPad Prism version 5.0.

Spontaneously Fibrillizing αSyn Assay—The procedure for performing the Thioflavin T aggregation assay was described previously (40). The αSyn was prepared by centrifuging the recombinant protein through a 100 kDa spin filter to remove preformed oligomers (35). DJ-1 and Hsp31 purified from either *E. coli* or *Saccharomyces cerevisiae*, respectively, were incubated with αSyn (17.5 μM) for 5 days at 37 °C. Thioflavin T (20 μM), a fluorescent dye that emits a signal only when binding to β-sheet-containing protein aggregates, was included in the reaction to detect the fibrillar state of αSyn by a Spectrafluor Plus microplate reader (Tecan, Uppsala, Sweden) at 440 nm for the excitation and 490 nm for the emission wavelength.

Dilution Growth Assays

Plasmids (pAG415-GPD-*ccdB*-DsRed and pAG415-*GPD-Hsp31*-DsRed) were transformed into W303 αSyn-expressing strains with or without a genomic copy of the *HSP31* gene knocked out using the PEG/lithium acetate transformation method. Single colonies of transformants were grown in SD−Leu overnight, and the cells were washed, normalized, and grown in synthetic complete medium without leucine (SC−Leu) + raffinose (2%) to switch the carbon source. After incubating in the raffinose medium overnight, the cell number was normalized, and dilutions were aliquoted on an SD−Leu (suppressed expression) plate and SC−Leu with 2% raffinose and 2% galactose (induced expression) with 5-fold serial dilutions. The plates were incubated at 30 °C for 3 days.

Fluorescence Imaging of αSyn Localization

pESC-Leu *myc-Hsp31* and control empty vector were transformed into two copies of αSyn-expressing strain. The αSyn expression was induced by growing cells in synthetic minimum medium plus 2% raffinose and 2% galactose for 8 h. The live cells were visualized using a Nikon TE2000-U inverted fluorescence microscope with Nikon Plan apochromat ×60 (numerical aperture 1.4) oil immersion objective and YFP filters plus ×300 magnification. In order to differentiate the localization of protein, ~50 individual cells were randomly counted in multiple regions of interest for each set of experiments. The ratio of membrane to cytoplasmic localization of αSyn fluorescent fusion protein was presented as the mean from three independent sets of experiments.

MGO Addition and Microscopy

αSyn-expressing strains with or without the *HSP31* gene deleted were grown in liquid yeast extract/peptone dextrose medium and transferred into medium containing 2% galactose and MGO (0.5–2 mM) for 6 and 12 h. Cells were washed and subjected to confocal microscopy to observe αSyn foci formation. The presence of MGO inhibited the growth of cells for the initial 12 h and resulted in an equal growth rate between strains regardless of the *HSP31* gene deletion. Strains could not be grown in the presence of high concentrations of MGO (20 mM), so αSyn was induced for 10 h, and then MGO was added and incubated for another 2 h before confocal microscopy analysis.

Assessment of Intracellular ROS

Cells were harvested after the induction of αSyn expression for 12 h, and 5×10^6 cells were prepared for staining with dihydroethidium. Cells were suspended in 250 μl of 2.5 μg/ml dihydroethidium in PBS and incubated in the dark for 10 min. Cells were washed in the PBS and were subjected to fluorescence microscopy (excitation at 485 nm and emission at 520 nm) and flow cytometry with the FL-2 channel. FlowJo software was used to calculate median fluorescence intensity.

Prion Expression Experiments

W303 wild type strain was co-transformed with pAG424-*GAL*-PrD-Sup35-EYFP and pAG415-*GPD-HSP31*-DsRed. Single transformations were also performed using the same constructs and their corresponding control vector. Cells were grown at 30 °C in appropriate medium overnight (SD−Trp for pAG424, SD−Leu for pAG415, and SD−Trp−Leu for co-transformants), and protein expression was induced for 24 h in SC 2% raffinose and 2% galactose-containing medium at 30 °C. After induction, cells were subjected to fluorescence microscopy using a Nikon A1 confocal microscope with a Nikon Plan apochromat ×60 (numerical aperture 1.4) oil immersion objective to acquire fluorescence and differential interference contrast images and were analyzed using ImageJ. Cultures identical to those used in microscopy were used to prepare samples for flow cytometry, and cells were washed and resuspended in PBS at a density of ~10×10^6 cells/ml. Cells were filtered and ana-

lyzed for EYFP fluorescence intensity using a flow cytometer with the FL-1 channel. A total of 10,000 events were acquired for each sample, and data were analyzed using FlowJo software to calculate median fluorescence intensity after three biological replicates.

Glutathione-independent Glyoxalase Biochemical Assay

Purified recombinant Hsp31 and Hsp31 C138D with the GST tag removed were used to assay methylglyoxalase activities. The reaction was initiated by adding the specified concentration of proteins (1 μM Hsp31 and 5 μM Hsp31C138D) in reaction buffer (100 mM HEPES, pH 7.5, 50 mM KCl, 2 mM DTT) to a 6 mM initial concentration of MGO (Sigma; 40% solution), followed by incubation at 30 °C. The assay was performed by removing 50-μl aliquots of the reaction at fixed time points (15, 30, 45, and 120 s) after the addition of protein. The amount of D-lactic acid produced by Hsp31 as a result of MGO consumption was measured. The initial rate obtained was divided by the amount of protein in the reaction mixture to calculate the specific activity. Samples were also subjected to gas chromatography-mass spectroscopy analysis (Agilent 5975C MSD) to identify the presence of D-lactic acid. Samples were derivatized with *N*,*O*-bis(trimethylsilyl) trifluoroacetamide) and trimethylchlorosilane and heated to 50 °C for 10 min and run in the electron impact mode with scanning from 42 to 400 atomic mass units. A lactic acid standard displayed a peak at 6.09 min identical to the peak detected in the Hsp31-treated sample, whereas Hsp31C138D did not display this peak. The spectral scan was visualized and displayed using the OpenChrom software (41). To obtain the enzymatic parameters, the reaction was initiated as described above by adding 1 μM Hsp31 or 5 μM Hsp31C138D protein into reaction buffer, and reactions were stopped after 1 min by heating at 85 °C for 30 s. A range of MGO substrate from 50 μM to 2 mM and the EnzyFluo D-lactate assay kit (Bioassay Systems) were used to determine the amount of D-lactic acid produced in each reaction. Each rate was determined in triplicate, and mean values were plotted to obtain enzymatic parameters (V_{max} and K_m) by fitting to a Michaelis-Menten model using GraphPad Prism.

Semidenaturing Detergent-Agarose Gel Electrophoresis (SDD-AGE)

W303 cells harboring pAG424-*GAL*-cPrDSup35-EYFP and pAG415-*GPD-HSP31*-DsRed plasmids were used, and aggregates were produced by inducing for 24 h in SC 2% raffinose + 2% galactose medium. Prion aggregates were analyzed using SDD-AGE (42). Briefly, to prepare lysates, cells were harvested by centrifugation at 3,000 × *g* for 2 min and resuspended in spheroplast solution (1.2 M D-sorbitol, 0.5 mM $MgCl_2$, 20 mM Tris (pH 7.5), 50 mM β-mercaptoethanol, and 0.5 mg/ml Zymolyase) and incubated at 30 °C for 30 min with shaking. After spheroplast formation, the samples were centrifuged at 800 rpm for 5 min at room temperature, and supernatant was removed. The pelleted spheroplasts were resuspended into 100 μl of lysis buffer (100 mM Tris, pH 7.5, 50 mM NaCl, 10 mM β-mercaptoethanol, and protease inhibitor) and vortexed at high speed for 2 min. The lysates were collected and mixed with 4× sample buffer (2× TAE, 20% glycerol, 4% SDS, 0.01% bromphenol blue). The samples were incubated at room temperature for 15 min and loaded onto a 1.8% agarose gel containing 1× TAE and 0.1% SDS and run at 50 V, followed by transfer onto nitrocellulose membrane using the capillary transfer method. The nitrocellulose membrane was subjected to Western blot analysis using anti-GFP antibody (Roche Applied Science). A strain harboring p2HG-Hsp104 plasmid was included as a positive control.

Results

Hsp31 Has Chaperone Activity—The *S. cerevisiae* open reading frame (*YDR533C*) has been assigned the name *HSP31*; however, direct functional studies demonstrating chaperone activity have not been conducted on this protein to support its designation within the HSP family. Hsp31, human DJ-1, and hchA are members of the ThiJ/DJ-1 superfamily based on similarity in structure, so we directly compared the *in vitro* chaperone activity between these proteins. The influence of Hsp31 on the aggregation of substrate proteins was measured using three different model substrates: CS, insulin, and αSyn. CS has been used as a classical substrate for *in vitro* chaperone assays, and both DJ-1 and hchA have demonstrated an ability to suppress CS aggregation (9, 43). To assess the chaperone activity of Hsp31, we purified the protein from yeast using the BG1805 plasmid-based system from the yeast movable ORF (MORF) collection (33). The C terminus of the protein retains a 4.8-kDa tag, as confirmed by mass spectrometry, and includes a His_6 and HA tag (see the amino acid sequence under "Experimental Procedures"). We also expressed Hsp31 with a GST tag fused to its N terminus using the pGEX-6p1 plasmid in *E. coli*. The tag was removed by 3C protease, and only 3 amino acids (GPL) were retained on the recombinant Hsp31 protein, which was confirmed by mass spectrometry (data not shown). We determined that the purified proteins were folded correctly because they behaved as homodimers based on gel filtration chromatography (data not shown) and by analytical ultracentrifugation with a sedimentation coefficient of 3.7 S (Fig. 1*A*). The Hsp31-MORF, purified from yeast, can completely suppress the heat-induced aggregation of CS when present at a 1:1 molar ratio (Fig. 1*B*). BSA, which was added at a 6-fold molar excess concentration of CS, had a slight effect on suppressing CS aggregation in agreement with a previous study that reported BSA as having a mild chaperone effect in the CS aggregation assay (44). *E. coli* hchA suppressed CS aggregation in a dose-dependent manner, but the high concentration of 0.6 μM did not approach the considerably more efficient suppression of CS aggregation by Hsp31-MORF (Fig. 1*B*). In addition, recombinant yeast Hsp31 purified from *E. coli* did not have activity at a 1:1 molar ratio and was needed at high molar ratios similar to hchA (data not shown) (Fig. 1*B*). In conclusion, Hsp31 purified from yeast can suppress CS aggregation at a 1:1 molar ratio, whereas hchA is needed at a 6:1 molar ratio to generate an appreciable suppression of aggregation. These results are consistent with previous studies, where high molar ratios of hchA were required in CS assays (38, 45).

To further characterize the chaperone activity of Hsp31, additional protein substrates were studied. Hsp31-MORF suppressed insulin aggregation induced by reducing agent, when

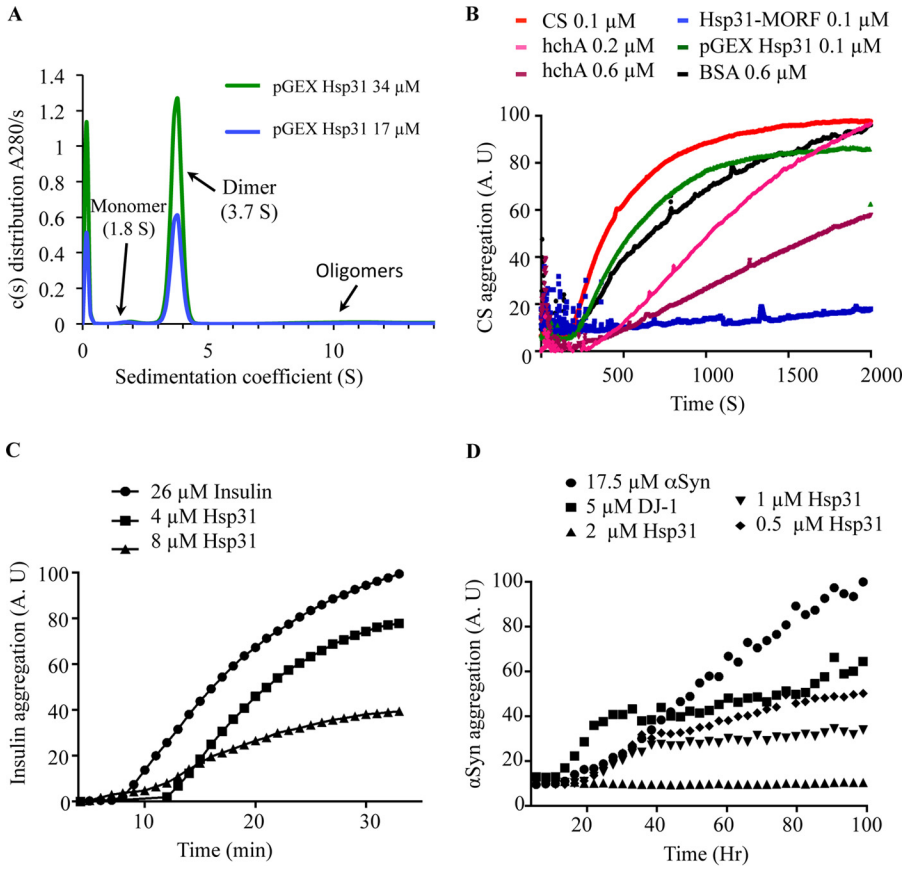

FIGURE 1. **Hsp31 inhibits *in vitro* protein aggregation of a variety of substrates.** *A*, the predominant form of Hsp31 is a homodimer in solution. Hsp31 was purified from the pGEX *E. coli* expression plasmid, and the GST tag was proteolytically removed. Sedimentation velocity was performed, and the *c*(*s*) distribution plot demonstrated that the majority species at 3.7 S is a dimeric protein. *B*, Hsp31 inhibited CS aggregation. CS at 0.1 μM reached a maximum aggregation (100%) after 30 min of incubation at 43 °C (*red*). The presence of Hsp31 purified using the MORF yeast expression plasmid suppressed CS aggregation (*blue*), but recombinant Hsp31, purified from the pGEX *E. coli* expression plasmid (*green*) with the GST tag removed, had a reduced effect. *E. coli hchA* was used as a positive control (0.2 μM (*pink*) and 0.6 μM (*purple*)) and had less anti-aggregation effect when compared with Hsp31-MORF. BSA, a negative control, had a slight anti-aggregation effect but was used at higher protein concentrations (*black*). Each *curve* is the average of three independent experiments. *C*, Hsp31 suppressed aggregation of insulin induced by reducing agent. The amount of 26 μM insulin aggregation after a 30-min incubation with 20 mM DTT was used to set the 100% aggregation arbitrary units (*A.U.*) (●). The presence of Hsp31 suppressed insulin aggregation (4 μM (■) and 8 μM (▲)). *D*, Hsp31 suppressed αSyn fibrillization. αSyn alone (●) was considered to be 100% aggregated after 100 h of incubation. Inhibition of αSyn fibrillization by Hsp31 was dose-dependent (2 μM (▲), 1 μM (▼), and 0.5 μM (◆)). DJ-1 (5 μM) (■) was used as the positive control in the assay. These data are representative of more than five independent experiments with all experiments demonstrating similar trends.

using a 3–6-fold molar excess of insulin (Fig. 1*C*), further establishing its chaperone activity in another commonly used chaperone assay. The mechanism of αSyn aggregation is unclear, and DJ-1 has been reported to decrease αSyn aggregates or cytoplasmic foci *in vitro* and *in vivo* (9, 14, 46, 47). Hsp31 completely suppressed αSyn fibrillization despite the presence of an 8-fold molar excess of αSyn and maintained chaperone activity when αSyn was present at a 35:1 molar ratio (Fig. 1*D*). In agreement with this result, we observed that DJ-1 suppressed αSyn fibrillization although not to the same extent as Hsp31. The difference may be due to the oxidation state of DJ-1, which has been shown to affect its activity (46). Taken together, these results demonstrate that Hsp31 has the ability to act as a chaperone in preventing several types of protein aggregation at substoichiometric concentrations.

Hsp31 Protects against αSyn Toxicity and Reduces αSyn Foci Formation and ROS Levels—Outeiro and Lindquist (23) demonstrated that two genomic copies of *GAL*-αSyn in yeast decreased cellular fitness, which was correlated with αSyn cellular aggregates (46). DJ-1 has been reported to alleviate protein aggregation (9, 46), and αSyn has been implicated as a factor in the progression of PD (48–50). To determine the chaperone effect of Hsp31 with its anti-aggregation activity and effect on cellular fitness, we tested the rescue of yeast cells from αSyn-mediated toxicity in dilution growth assays. Overexpression of one copy of the αSyn gene from the *GAL* (galactose) promoter had negligible effects on cellular fitness, but *GAL*-driven overexpression of two αSyn gene copies resulted in severe toxicity, confirming previous findings of dose-dependent toxicity. The αSyn toxicity was markedly alleviated in the presence of constitutive expression of Hsp31 (*pGPD-HSP31*), as evidenced by the full rescue of cell viability (Fig. 2*A*). In addition, we expressed one copy of *GAL*-αSyn in an *hsp31*Δ strain to determine whether there was a synthetic genetic interaction between these genes. Dilution growth assays demonstrated that expression of a single copy of αSyn or knocking-out *HSP31* alone was phenotypically similar to the wild-type strain with respect to viability. However, cellular fitness was significantly reduced when expressing a single copy of αSyn in the *hsp31*Δ strain (Fig. 2*B*). The synthetic lethal interaction of αSyn and deleted *HSP31*

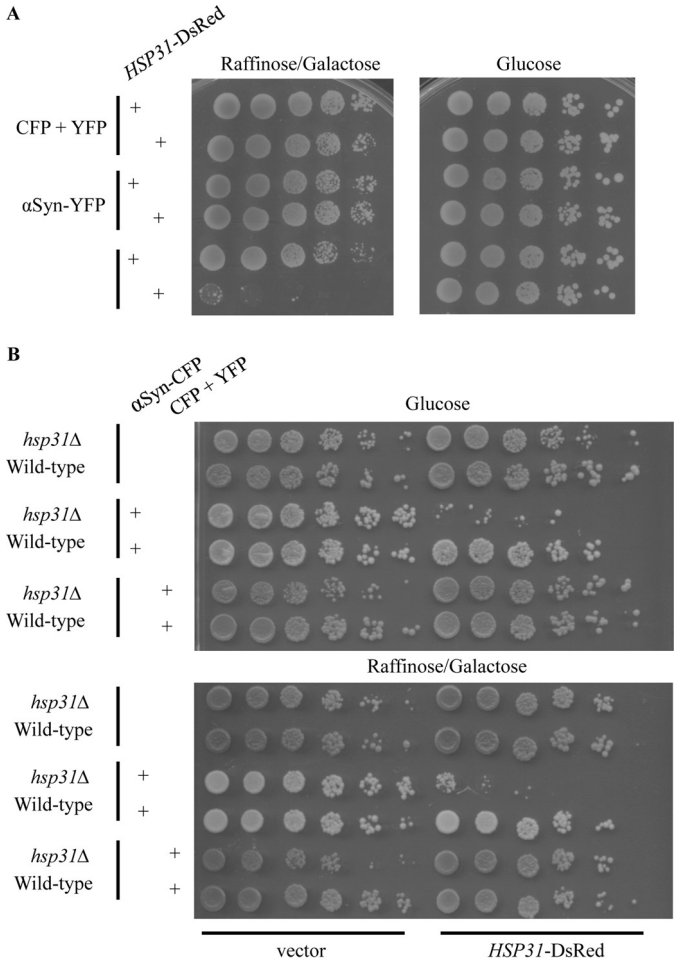

FIGURE 2. **Hsp31 rescues cells from αSyn mediated toxicity.** *A*, Hsp31 co-expression in yeast reduced αSyn toxicity. A yeast strain containing one or two copies of genomically expressed *GAL*-αSyn was used in a growth dilution assay, in the presence of p*GPD-HSP31*-DsRed or empty vector, in media containing galactose/raffinose (*left*) or glucose (*right*). The strain harboring two copies of the αSyn gene had better fitness when transformed with the *Hsp31*-encoding construct compared with the empty vector. *B*, combination of *hsp31*Δ with single copy αSyn expression is toxic for yeast. The expression of a single copy of αSyn in *hsp31*Δ strain reduced cellular fitness in the presence of glucose (*top*) and raffinose/galactose (*bottom*). The overexpression of Hsp31 in the same strain was able to rescue viability on both types of media.

using this approach provided further evidence that Hsp31 is a molecular chaperone with the ability to protect cells from αSyn-mediated toxicity.

Previous studies demonstrated that the subcellular localization of αSyn changed from the plasma membrane to cytoplasmic foci with increased expression of αSyn in yeast cells (23). Using this relocalization property, we examined the effect of p*GAL HSP31* overexpression in altering the distinctive subcellular localization profile of 2x*GAL*-αSyn. The same strains used in the dilution growth assay were used to monitor the effect of Hsp31 expression on αSyn localization. We quantified the number of cells with specific localization profiles at 8 h postinduction and observed that 60% of cells exhibited αSyn foci when only expressing αSyn, but only 33% of cells co-expressing αSyn and Hsp31 contained foci (Fig. 3, *A* and *B*). We observed that the suppression of αSyn foci by p*GAL HSP31* was transient because 24 h after induction, the percentage of cells with foci increased and was similar to the percentage observed for cells expressing αSyn alone. This result is consistent with our rescue experiments, which were only successful when *HSP31* was expressed from the *GPD* promoter (Fig. 2, *A* and *B*) and not when expressed from the *GAL* promoter (data not shown).

The expression of αSyn has been demonstrated to increase the level of ROS in yeast (51). The *in vivo* suppression of αSyn foci by Hsp31 and increased toxicity of one copy αSyn in the *hsp31*Δ strain prompted us to investigate the level of ROS in these different genetic contexts. We found that wild-type yeast did not have detectable superoxide radicals when treated with dihydroethidium using microscopy and a fluorescence level of 0.5 arbitrary units by flow cytometry (Fig. 3, *C* and *D*). ROS levels were detectable in a fraction of cells in the *hsp31*Δ strain (6 arbitrary units), indicating that the presence of Hsp31 in the cell can decrease ROS levels of normal cells not expressing αSyn. The remaining strains had increased ROS levels in the following order: αSyn-YFP strain (23 arbitrary units), αSyn-YFP *hsp31*Δ (41 arbitrary units), αSyn-YFP αSyn-CFP (64 arbitrary units), and αSyn-YFP αSyn-CFP *hsp31*Δ (133 arbitrary units). The latter three strains with the highest ROS levels exhibit reduced viability when αSyn is expressed and form increased foci, demonstrating a correlation between these phenotypes.

Hsp31 Is an Integral Part of the Yeast Cellular Stress Response—Multiple studies have shown that environmental stresses, such as oxidative stress and increasing temperature, increase the expression of Hsp31 (26, 52). A recent study demonstrated increased *HSP31* mRNA levels upon treatment with H_2O_2, during the diauxic shift growth phase and stationary phase (22). However, the Hsp31 protein level was not characterized under these conditions. We generated a yeast strain with a genomically integrated 9myc epitope at the C terminus of the *HSP31* locus to quantify protein expression. We examined Hsp31 protein expression levels during growth in rich media relative to optical density and demonstrated that Hsp31 expression could be divided into three phases. We found that Hsp31 expression decreased during log phase and then reached maximum expression during early stationary phase relative to the cell density of the culture and remained at approximately the same level in stationary phase when cell density was saturated after growth for 24 h (Fig. 4*A*). This distinctive expression pattern results in the initiation of elevated expression of Hsp31 corresponding to the diauxic shift, which occurs between log phase and stationary phase (26). To assess whether Hsp31 expression increases under other stress conditions, we exposed cells to H_2O_2 and observed increased protein expression within 1 h of exposure (Fig. 4*B*). This increased expression in response to an ROS-inducing agent has been observed previously (22, 26).

We also examined the expression profile of Hsp31 to a proteotoxic stress in the form of αSyn overexpression, and the results indicated that increased expression of αSyn decreases cell viability and concomitantly increases the expression of Hsp31 during log phase compared with a strain not expressing αSyn (Fig. 4, *C–E*). The characteristic decrease in expression during log phase, 6–9 h postinoculation, is not observed when αSyn is expressed. Our data demonstrate that Hsp31 expression is rapidly elevated at the protein level in the event of

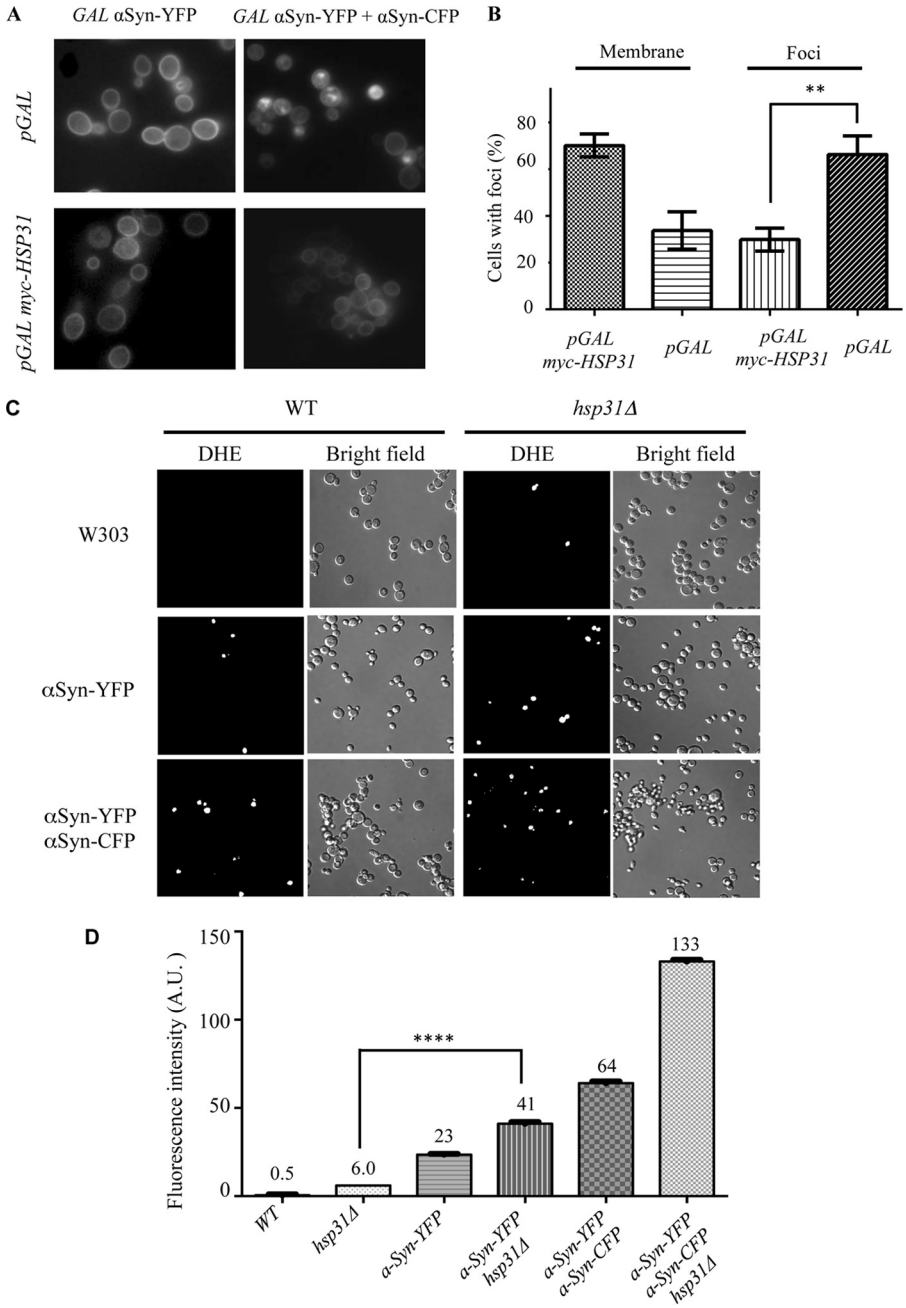

FIGURE 3. **Hsp31 alters the subcellular localization of αSyn and decreases ROS generated by αSyn.** *A*, single copy of CFP-tagged αSyn localized mainly to plasma membrane (*top left*). Cytoplasmic foci predominate when two copies of αSyn are expressed (*top right*). Co-expression of p*GAL-HSP31* with *GAL*-αSyn did not change the localization of αSyn when one copy of the gene was expressed (*bottom left*) but significantly reduced foci formation when two copies of αSyn were expressed (*bottom right*). *B*, quantification of microscopic images demonstrates that Hsp31 alters the subcellular localization of αSyn. The percentage of cells with αSyn localizing to the membrane when Hsp31 is present is greater in αSyn-expressing cells transformed with the Hsp31-encoding construct *versus* the control vector. This experiment was done at 8 h postinduction, and cells with one or more foci were counted in a blinded manner ($n \geq 100$ cells/sample; **, $p \leq 0.01$ determined by *t* test; $p = 0.0013$). The *column bars* represent the means of the three independent biological replicates. *Error bars*, S.D. *C*, superoxide ions increase when *HSP31* is deleted and when αSyn is expressed. The *in vivo* presence of superoxide ions was detected by treatment with dihydroethidium and visualization by fluorescence microscopy. Representative fields of view are presented. *D*, quantification of superoxide ion increase in *hsp31*Δ- and *GAL*-αSyn-expressing strains. Flow cytometry was performed on three biological replicates. ****, $p \leq 0.0001$ based on one-way analysis of variance with multiple comparison *t* test. *A.U.*, arbitrary units. *Error bars*, S.D.

growth stress associated with diauxic shift, oxidative stress, and proteotoxicity.

Hsp31 Methylglyoxalase Activity Is Not Required for Rescue of αSyn-mediated Toxicity—Recent studies have shown that DJ-1 and Hsp31 are methylglyoxalases that convert MGO into D-lactate in a single step independent of GSH (53, 54). Hsp31, like other members of the DJ-1 superfamily, possesses the conserved Glu-Cys-His catalytic triad (18). The first two residues of this triad are critical for MGO activity of DJ-1 as well as Hsp31 in *Schizosaccharomyces pombe* (54). We determined the methylglyoxalase activity for recombinant Hsp31 (purified from *E. coli* with the GST tag removed to retain 3 amino acids, GPL, on the C terminus) and a catalytic triad mutant, Hsp31 C138D, using a commercially available D-lactate assay kit. As expected,

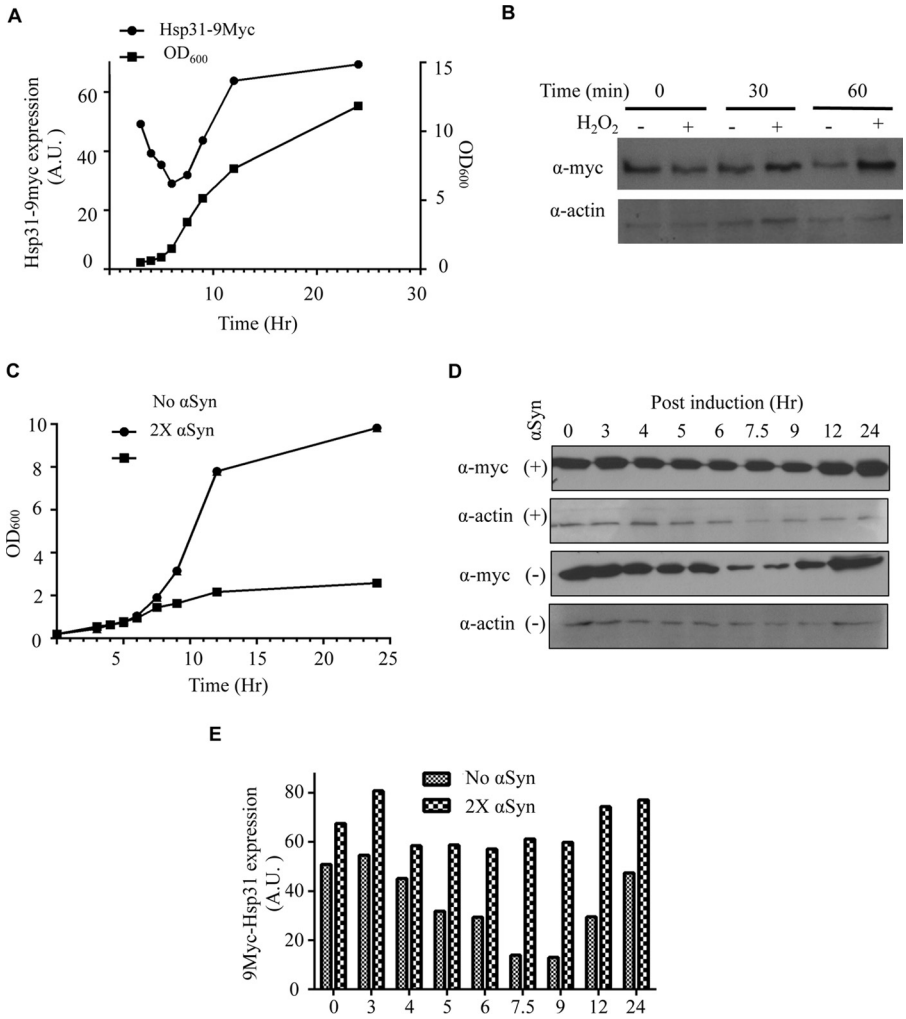

FIGURE 4. **Hsp31 expression increases at early stationary phase, under oxidizing conditions, and with αSyn expression.** *A*, Hsp31 reached maximal expression at early stationary phase. Cell growth curves are represented by A_{600} values (■). Cells were normalized to A_{600} = 0.2 at the start, and aliquots were collected until stationary phase was reached ~12 h postinoculation and at 24 h when the culture was saturated. The expression of genomically tagged Hsp31-9myc expression was assessed via immunoblot analysis of cell lysates obtained at corresponding time points. The plot shows expression levels normalized to β-actin levels (●). *B*, H_2O_2 treatment increases the expression of Hsp31. The Hsp31–9myc strain was exposed to 1 mM H_2O_2 treatment for 30 and 60 min, and increased Hsp31 expression was determined by immunoblot. Samples were normalized for cellular density by A_{600}, and β-actin was used as a loading control. These data are representative of three independent experiments. *C*, growth curves showing the inhibitory effect of *GAL*-αSyn expression in yeast harboring two copies of αSyn. Cells were normalized to A_{600} = 0.2 at hour 0, representing the time of inoculation, and the OD was monitored for 24 h at the identical time points used in *A*. Cells containing two copies of genomically integrated αSyn (■) grew more slowly 9 h after inoculation compared with the same strain without αSyn (●). *D*, Hsp31–9myc expression increased in the presence of induced *GAL*-αSyn. The immunoblot was probed with anti-Myc and anti-β-actin antibodies. The level of Hsp31 at the 7.5 and 9 h time points did not decrease in the 2xαSyn strain compared with the strain that did not express αSyn. *E*, quantitation of Hsp31 expression level reveals increased expression during log phase. The Hsp31–9myc-tagged cells with and without two copies of αSyn were harvested at 0, 3, 4, 5, 6, 7.5, 9, 12, and 24 h after inoculation. The levels of Hsp31 expression were quantified and normalized to the β-actin signal. Three independent experiments were performed, and all experiments resulted in similar trends as observed here. *A.U.*, arbitrary units.

Hsp31 could convert MGO into D-lactate with a calculated specific activity of 28.4 μmol/min/mg enzyme (using a saturating substrate concentration of MGO at 6 mM). These enzymatic parameters indicate a more efficient enzyme activity than the previously reported Hsp31-specific activity of 10.5 D-lactate μmol/min/mg (53). The Hsp31-MORF purified from yeast had similar enzymatic parameters as the recombinant Hsp31 (data not shown). Enzymatic parameters were calculated by measuring the time-dependent production of D-lactate with varying substrate concentrations and fitting to a Michaelis-Menten kinetics model, resulting in a V_{max} of 0.0356 μmol of D-lactic acid/min (S.E. = 0.0016), and K_m was 247.4 μM (S.E. = 31.5) (Fig. 5*A*). Specific activity for the mutant could not be determined because low levels of D-lactate were produced despite using 5 times the amount of protein (detection limit of 0.4 μmol/min/mg). The reaction products of these assays were examined by GC-MS, and a peak identical to the lactic acid standard (6.09-min elution time) was identified, confirming the production of lactic acid by Hsp31 (Fig. 5*B*). Lactic acid was undetectable by GC-MS analysis in the Hsp31 C138D sample (data not shown).

We next determined whether methylglyoxalase activity is required for rescue of αSyn toxicity. One copy of αSyn-YFP decreases fitness in the *hsp31*Δ strain, but *GPD*-driven expression of Hsp31 rescues that toxicity. The expression of *GPD*-driven Hsp31 C138D restored the αSyn-expressing strain to full viability comparable with expression of the wild-type Hsp31 (Fig. 5*C*). The lack of enzyme activity for this mutant and the

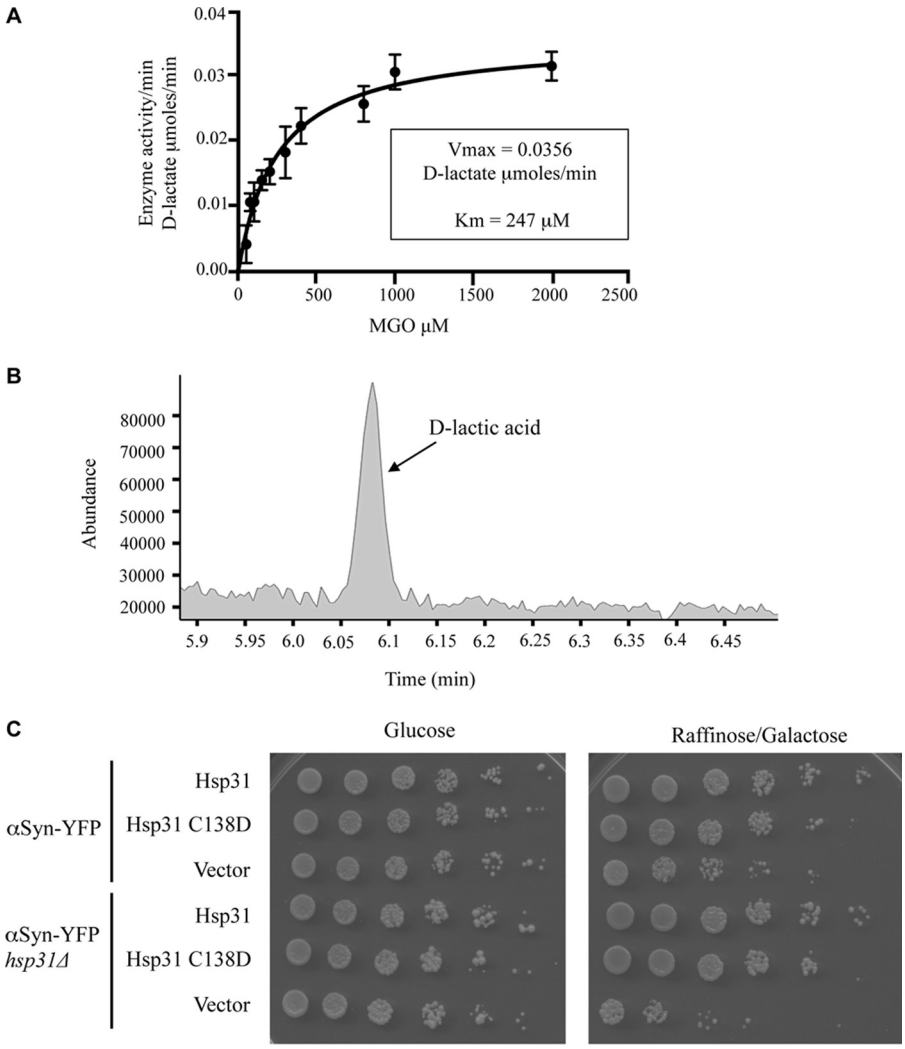

FIGURE 5. **Hsp31 is a methylglyoxalase that produces D-lactic acid, and the enzyme activity is not necessary for rescuing αSyn toxicity.** *A*, the plot of substrate concentration *versus* rate of D-lactate production by Hsp31 is depicted, and the Michaelis-Menten best fit model is represented by the *solid line*; V_{max} and K_m were determined based on this model. Mean values of triplicate experiments are plotted. *Error bars*, S.D. *B*, GC-MS trace demonstrates a peak (6.09 min) consistent with the production of D-lactic acid by Hsp31 in the enzymatic reaction. *C*, overexpression of p*GPD HSP31* or the C138D mutant rescues toxicity from αSyn-expressing strains.

ability to rescue αSyn toxicity indicated that the *in vivo* mechanism of rescue is not dependent on methylglyoxalase activity.

MGO is a toxic metabolite produced during glycolysis (53–55) that reacts with proteins to yield toxic advanced glycation end products (56, 57) and has been associated with increased αSyn cross-linking and formation of intracellular foci formation in neuroblastoma cells (58). We examined whether increased levels of MGO could increase the αSyn foci or toxicity by treating cells with exogenous MGO and found no increased foci in wild-type yeast, indicating that their formation is probably not influenced by MGO. In addition, the *hsp31*Δ strain also did not have increased foci, suggesting that lack of Hsp31 is not sufficient to increase foci formation due to MGO treatment (Fig. 6, *A* and *B*). We determined that MGO was toxic to wild-type yeast at 10 and 20 mM MGO, and viability in the *hsp31*Δ strains was similar to wild type, suggesting that Hsp31 is not sufficient for detoxification. The concomitant expression of αSyn (one or two copies) and treatment with MGO did not have differential effects on viability (Fig. 6*C*). Consistent with these results is that cell lysates of the *hsp31*Δ strain had levels of overall methylglyoxalase activity equivalent with those of wild type because other yeast methylgloxalase enzymes, Glo1 and Glo2, are present in yeast and have been shown to detoxify MGO (59, 60) (data not shown).

Hsp31 and Catalytic Triad Mutants Prevent the Transition of αSyn Monomers to SDS-resistant Oligomeric Species—The demonstrated chaperone activity of Hsp31 prompted us to investigate at what stage Hsp31 prevents protein aggregation. We used the spontaneous *in vitro* fibrillization of αSyn assay as a method to investigate the different oligomeric species in the presence of Hsp31. The prolonged incubation of recombinant monomeric αSyn results in fibrillization and precipitation of the protein. Fractionation of the precipitate *versus* supernatant and subsequent electrophoresis on SDS-PAGE allowed the detection of different oligomeric species that appear to be SDS-resistant (Fig. 7*A*). The αSyn higher order oligomers were reduced in the pellet fraction and nearly non-existent in the supernatant when Hsp31 wild-type and catalytic triad mutants

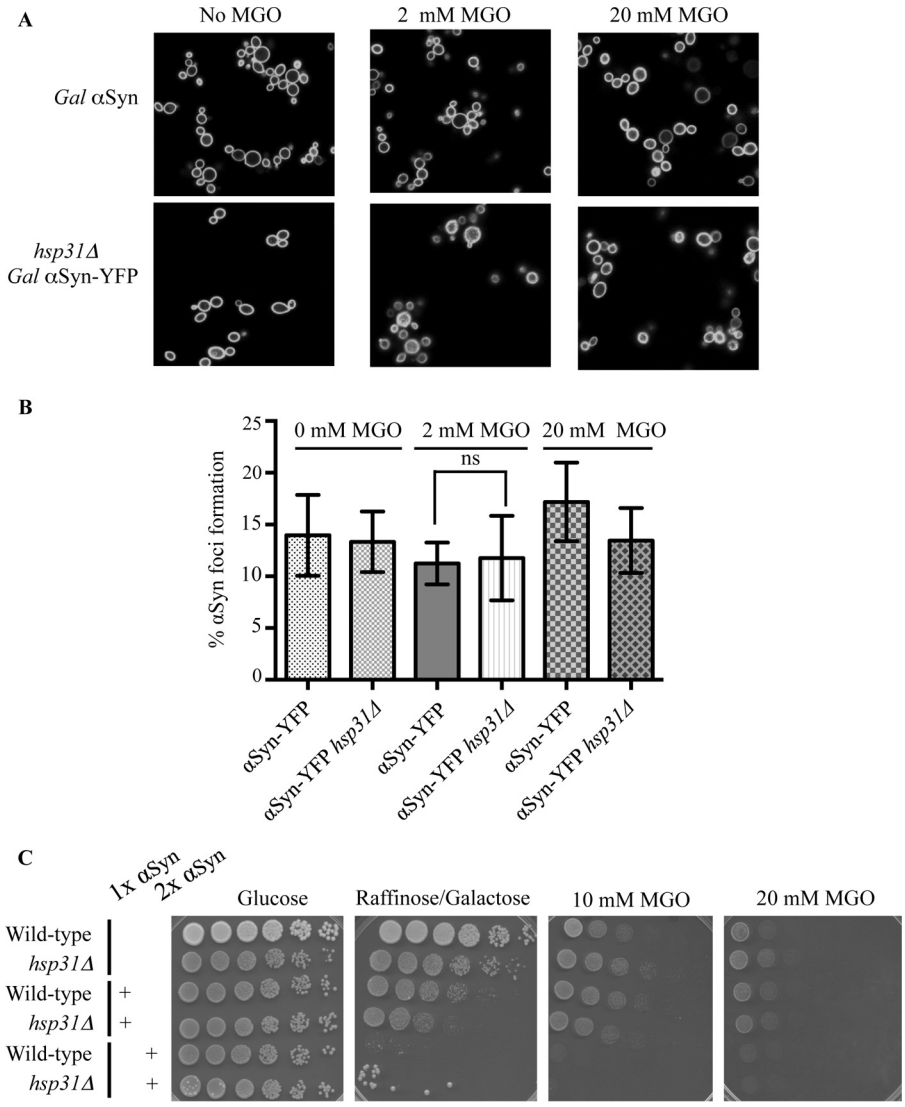

FIGURE 6. **MGO does not increase αSyn foci or toxicity.** *A*, representative fluorescence microscopy images of αSyn-expressing cells treated with 2 and 20 mM MGO. *B*, the level of αSyn foci does not increase with MGO treatment. Percentage of cells with αSyn foci formation was quantified for the two strains (αSyn-YFP and αSyn-YFP/Hsp31Δ) in the presence of 2 and 20 mM MGO. Cells in three or more fields of view were counted, and the mean values were plotted (*error bars*, S.D.). *Ns*, one-way analysis of variance with multiple comparison *t* test indicates no significant difference. *C*, MGO treatment does not differentially increase toxicity of αSyn-expressing strains compared with non-expressing counterparts. Strains were serially diluted on agar plates containing 10 and 20 mM MGO. *A.U.*, arbitrary units.

were present (Fig. 7*B*). The greatly reduced presence of soluble but SDS-resistant oligomers indicates that Hsp31 may interact with the monomer or an early oligomeric species to prevent formation of later stage oligomers. The same reactions were monitored using the ThioT assay, and only a baseline level of fluorescence was observed in the presence of Hsp31, further supporting the hypothesis that Hsp31 interacts with an αSyn species that precedes larger oligomers detected by ThioT (Fig. 7*C*). The ability of mutants to reduce fibrillization is consistent with our observation that the mutants suppress αSyn toxicity in yeast (Fig. 5*C*).

Hsp31 Prevents Formation of Large Prion Aggregates—The demonstration that Hsp31 possesses chaperone activity in a variety of anti-aggregation assays prompted us to investigate whether Hsp31 could also modulate the oligomeric state of yeast prion proteins, such as the Sup35 prion. The aggregation state of prions in living cells can be monitored by fusion of fluorescent protein tags to prion-forming domains (PrD), so we overexpressed Hsp31 to determine whether it modulated the aggregation of Sup35 PrD. Consistent with previous findings, cells overexpressing PrD in the presence of endogenous Sup35 showed characteristic ribbon-like or punctate aggregates, which were localized around the vacuoles and/or adjacent to plasma membranes (Fig. 8*A*). The number of cells co-expressing p*GPD-HSP31*-DsRed and p*GAL*-PrD-Sup35-EYFP had ~3-fold fewer Sup35 fluorescent aggregates compared with cells harboring p*GAL*-PrD-Sup35-EYFP plus vector control, indicating that Hsp31 can inhibit the formation of microscopically visible Sup35 prion aggregates (Fig. 8, *A* and *B*). The intrinsic fluorescence of Sup35-EYFP appears to increase upon aggregation, which allowed us to utilize flow cytometry as an alternative method to quantitatively measure and show decreased Sup35 aggregation (Fig. 8*C*). This phenomenon has not been exploited widely but was noted in at least one previous

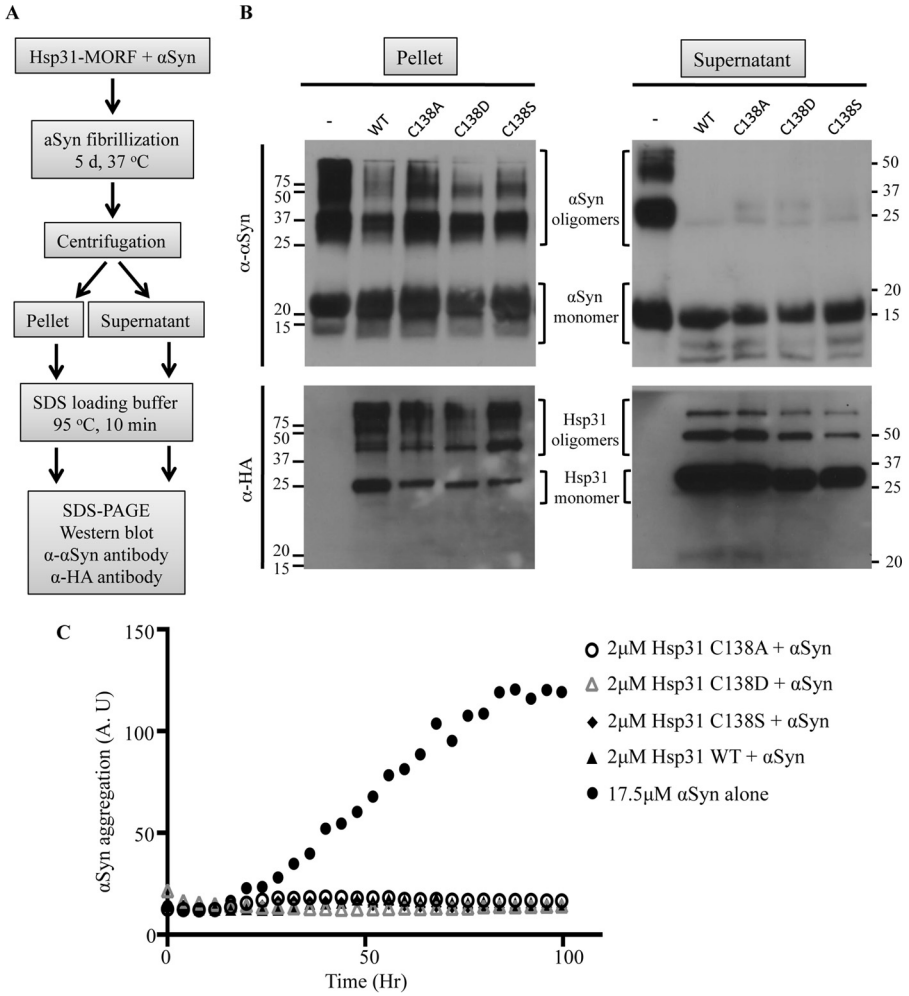

FIGURE 7. **Hsp31 and catalytic mutants prevent the formation of αSyn oligomers.** *A*, flow chart depicting the fractionation of the αSyn fibrillization assay and detection of monomeric and oligomeric species. SDS-PAGE of the pellet and supernatant fractions was performed, and antibodies were used to detect αSyn followed by stripping of the membrane and reprobing with anti-HA tag antibody to detect Hsp31 (note that Hsp31 was purified using the MORF tag, but Protein A was removed proteolytically, and the HA tag is retained). *B*, Hsp31 suppresses the formation of SDS-resistant higher order oligomers detected with Western blotting of the pellet and supernatant fractions. *C*, Hsp31 catalytic triad mutants suppress αSyn fibrillization. All proteins were added at the same level of 2 μM. *A.U.*, arbitrary units.

study investigating the aggregation of a huntingtin-GFP fusion protein (61). Cell cultures co-expressing Sup35 and Hsp31 used in the microscopy experiments were prepared for flow cytometry and analyzed for EYFP fluorescence intensity. The flow cytometry results were similar to the microscopy results because Hsp31-expressing cells consistently exhibited lower median Sup35-EYFP fluorescence intensity when compared with cells containing Sup35-EYFP expression plasmid and empty vector (Fig. 8*C*). Individual traces depicting the number of counting events for each yeast strain also show the decrease in cellular fluorescence intensity when Hsp31 is expressed (data not shown).

Expression of Hsp31 with the *GPD* promoter was diffuse and cytoplasmic and varied in intensity in individual cells across the total cell population. The cytoplasmic localization profile of Hsp31 was not altered when PrD-Sup35 was expressed (Fig. 8*A*). Interestingly, we observed overlapping localization in cells with Sup35 aggregates and relatively high levels of Hsp31, but the proteins do not appear to mutually co-localize (Fig. 9*A*). In some cells, it was evident that the DsRed signal was decreased in the area where there was a Sup35 aggregate, suggesting that Hsp31 is not incorporated in aggregates (Fig. 9*A*). The aggregate appears to occlude Hsp31, and the diffuse overlapping signal observed in some cells is consistent with the presence of Hsp31 throughout the cytoplasm surrounding the aggregate. We also confirmed that Hsp31 overexpression reduces the formation of *in vivo* aggregates based on assessing cell lysates by SDD-AGE. We found that SDS-resistant Sup35 aggregates were greatly reduced when Hsp31 was overexpressed. The positive control, Hsp104, completely eliminated detectable Sup35 aggregates (Fig. 9*B*). These results are consistent with the ability of Hsp31 to inhibit the formation of large protein aggregates.

We also ascertained whether other chaperones are induced upon overexpression of Hsp31. We demonstrated that Hsp70 and Hsp104 expression are not altered, and hence elevated expression of these chaperones is not responsible for the observed suppression of prion aggregates (Fig. 9*C*). This is in agreement with our *in vitro* aggregation studies establishing that purified and recombinant Hsp31 protein is solely sufficient

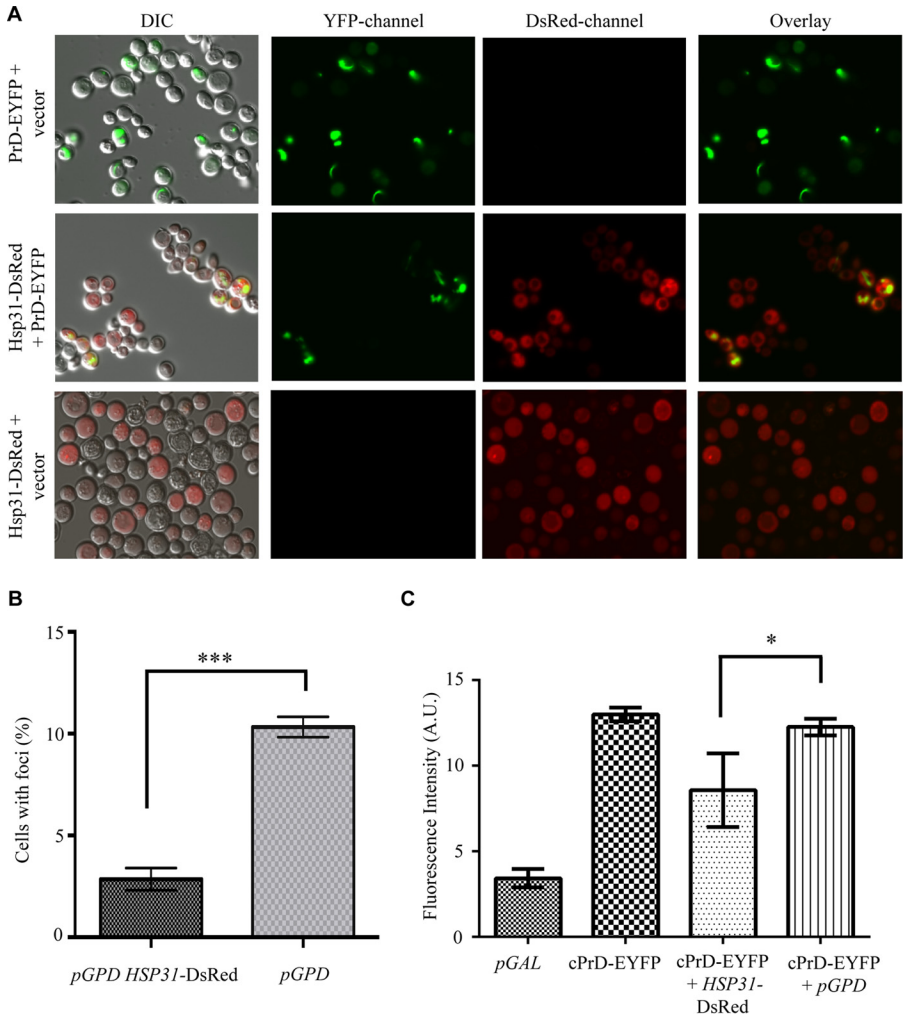

FIGURE 8. **Fluorescence microscopy demonstrating Hsp31 suppression of Sup35 aggregation.** *A*, PrD-Sup35 produced ribbon-like and punctate aggregates that are decreased when Hsp31 is overexpressed. PrD-Sup35-EYFP was overexpressed for 48 h at 30 °C in control W303 cells or W303 cells expressing elevated levels of Hsp31. Hsp31 was diffuse in the cytoplasm and decreased the presence of Sup35 aggregates. The diffuse cytoplasmic localization of Hsp31 did not appear to be altered as a result of Sup35 expression. *B*, quantitation of cells with one or more Sup35-EYFP foci. A smaller proportion of cells with Sup35 aggregates was evident in Hsp31-overexpressing cells compared with vector control (p*GPD*). Values represent mean ± S.E. ($n = 3$). ***, two-tailed Student's *t* test; $p \leq 0.001$. *C*, quantitation of Sup35-EYFP fluorescence suppression by Hsp31 using flow cytometry. Hsp31 overexpression lowers the median fluorescence intensity (*FI*; arbitrary units (*A.U.*)) of Sup35 compared with empty vector control. *, two-tailed Student's *t* test; $p \leq 0.05$). *Error bars*, S.E.; $n = 3$ biological replicates. *DIC*, differential interference contrast.

to prevent protein aggregation, although we cannot exclude the possibility that Hsp31 could collaborate with other chaperones to prevent prion aggregation in the cell.

Hsp31 Rescue of αSyn-mediated Toxicity Is Independent of the Autophagy Pathway—Recently, in several studies, autophagy has been identified as one of the main mechanisms to clear and recycle misfolded proteins and aggregates in the cytosol (62, 63). In addition to the ubiquitin proteasome system, autophagy is a major cellular function involved in clearance of misfolded and aggregated proteins, including αSyn aggregates (62). Deletion of autophagy genes, such as *ATG5* or *ATG7*, leads to neurodegenerative disease in mice (64, 65). In yeast, deletion of the *ATG1* gene reduced the clearance of αSyn aggregates (66). Deletion of *HSP31* was also demonstrated to impair autophagy under carbon starvation conditions (22). These studies raise the possibility that Hsp31 could be promoting autophagy of aggregated protein. In order to exclude the possibility that the Hsp31 rescue effect on αSyn toxicity depends on autophagy, we deleted the *ATG8* gene in the αSyn strains and assessed the synthetic lethal effects of αSyn expression in these strains. As expected, expression of αSyn in the *atg8*Δ strain resulted in decreased viability compared with the wild-type strain. The *atg8*Δ *hsp31*Δ strain had viability similar to that of the *atg8*Δ strain when αSyn was expressed (Fig. 10*A*). These results confirm that autophagy is a protective mechanism against αSyn toxicity. The lack of synthetic lethal defect between *ATG8* and *HSP31* with and without αSyn expression is consistent with genes that are in the same pathway and hence do not buffer each other. Expression of Hsp31 and the C138D mutant in the autophagy strains, *atg8*Δ αSyn or *atg8*Δ *hsp31*Δ αSyn, increased viability in rich YEP media compared with vector controls (Fig. 10*B*). We found that the rescue effect in synthetic media was not easily observed because expression of αSyn was not toxic in the *atg8*Δ strain background, but it was toxic in the *hsp31*Δ, indicating that media conditions are an important factor in this complex relationship (Fig. 10*B*, *mid-*

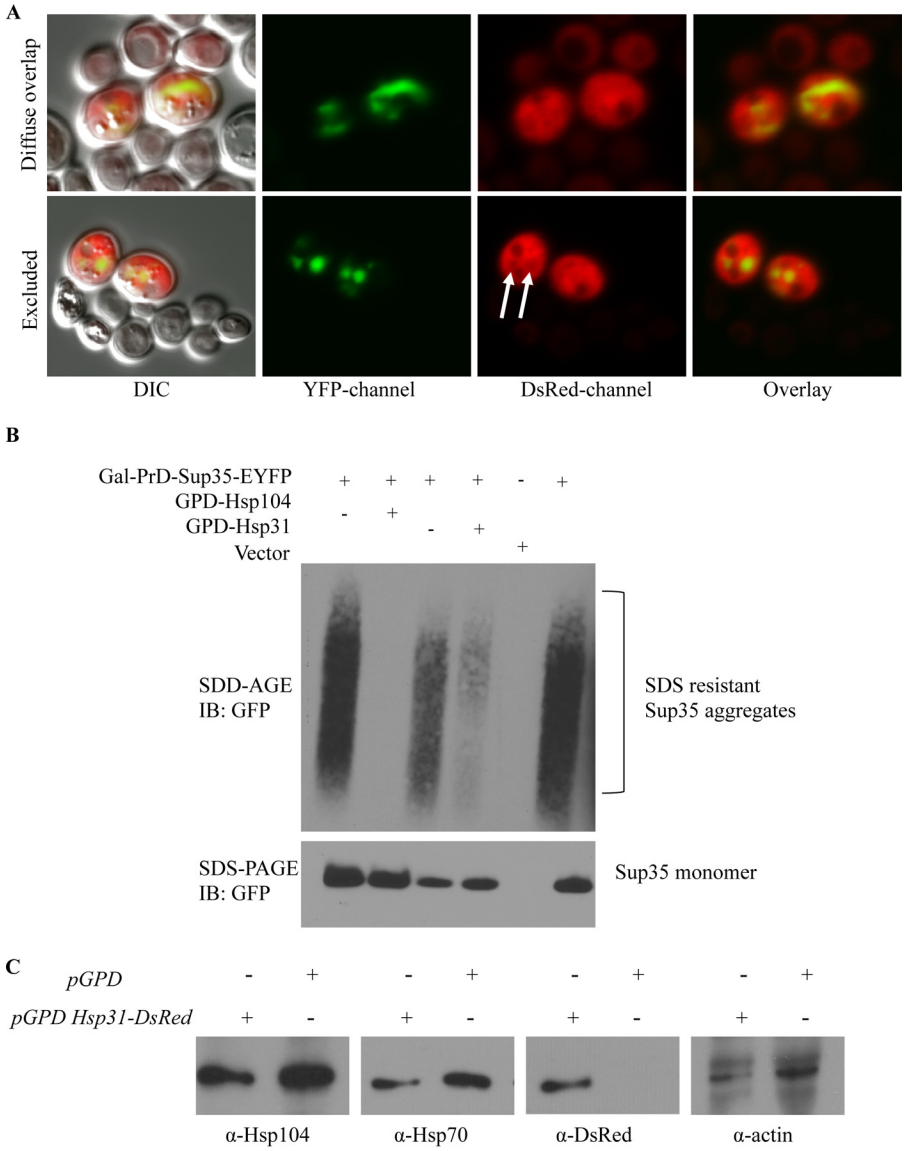

FIGURE 9. **Hsp31 and Sup35 are not mutually co-localized, and Hsp104 and Hsp70 are not altered.** *A*, most cells with high levels of expression of Hsp31 and Sup35 exhibited diffuse cytoplasmic localization for Hsp31 that overlapped with Sup35 (*top*). Occlusion of Hsp31 from the Sup35 aggregate was also observed, as evidenced by the decreased DsRed signal at aggregate sites (*white arrows*, *bottom panel*). *B*, SDS-resistant Sup35 aggregates are suppressed by Hsp31. Cellular lysates were subjected to SDD-AGE and SDS-PAGE. Overexpression of Sup35-PrD-EYFP initiated the formation of Sup35 aggregates, which were detected with anti-GFP antibody. *C*, Hsp31 overexpression does not alter the expression levels of Hsp104 and Hsp70. Cells of the BY4741 strain harboring the *pGPD-HSP31-DsRed* or vector control (*pGPD*) were grown overnight, and samples were prepared as described in the legend to Fig. 3. Immunoblots (*IB*) were probed with anti-Hsp104, anti-Hsp70, anti-DsRed, and anti-actin antibodies.

dle). These results demonstrate that Hsp31 can rescue αSyn toxicity in autophagy-deficient cells.

Discussion

The roles of chaperones and proteases in maintaining integrity and activity of folded, partially folded, and misfolded proteins are well established. Members of the DJ-1/ThiJ/PfpI superfamily exist in prokaryotes and eukaryotes, and structural and biochemical analyses have established that they have multiple activities, including chaperone, protease, and enzymatic functions. Because of the multiple activities associated with this superfamily, we sought to characterize the chaperone activity of Hsp31 and delineate its contribution in protecting against cellular stress.

The crystal structure of yeast Hsp31 has been solved, and structural evidence shows that Hsp31 and hchA share high similarity, in terms of the position of a hydrophobic patch and a catalytic triad. Yeast Hsp31, *E. coli* hchA, and human DJ-1 are in the same DJ-1/PfpI/ThiJ superfamily, and the literature suggests that both DJ-1 and hchA have chaperone-like effects against protein aggregation. Despite these similarities, the structures differ in important details, and it could have been argued that Hsp31 might not possess chaperone activity based on the absence of 45 amino acids present in hchA and the distinct dimerization. We investigated whether the chaperone-like activities are conserved in Hsp31 and found that the protein showed broad chaperone activity on three different substrate proteins, with aggregation induced by different mechanisms.

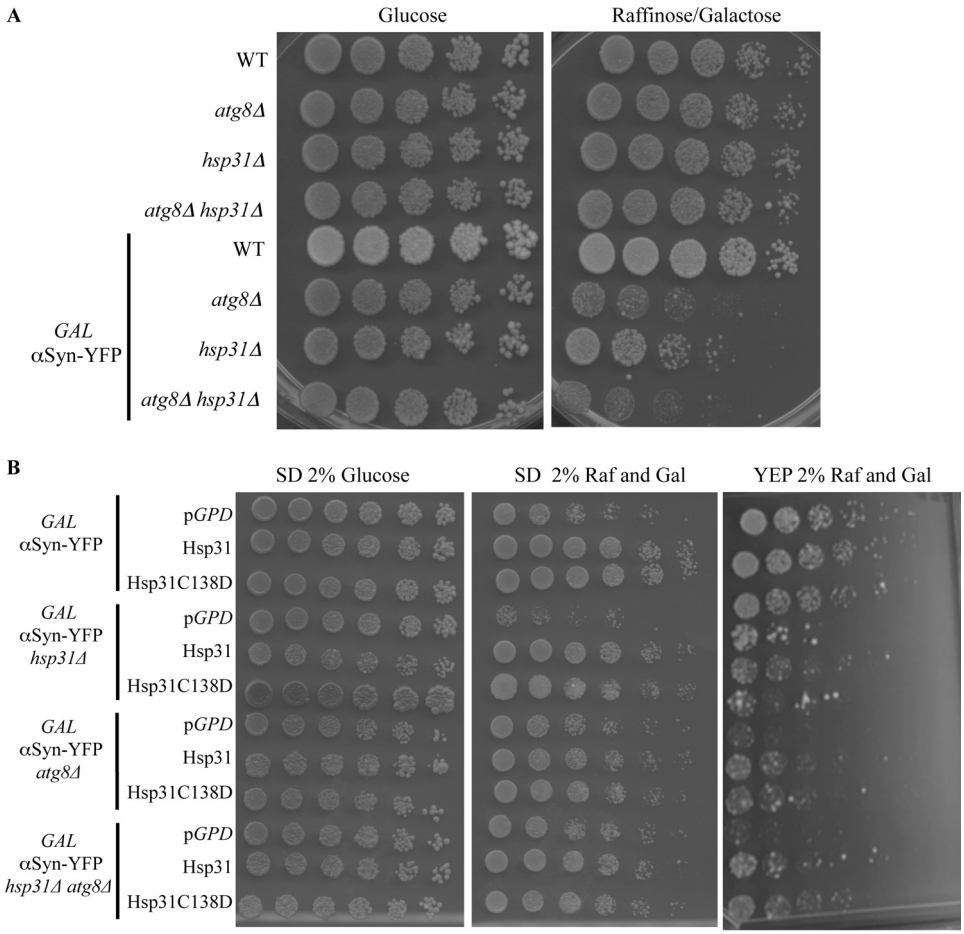

FIGURE 10. **The autophagy pathway prevents αSyn toxicity but is not required for Hsp31-mediated rescue.** *A*, yeast strains serially diluted on YEP agar plates (glucose or raffinose/galactose) demonstrating the toxicity of *GAL*-αSyn in the *atg8*Δ, *hsp31*Δ, and *atg8*Δ *hsp31*Δ strains. *B*, overexpression of *HSP31* using pAG415-*GPD-HSP31*-DsRed or the C138D mutant partially rescued toxicity of αSyn expression on YEP media for the *atg8*Δ, *hsp31*Δ, and *atg8*Δ *hsp31*Δ strains (*right*). Rescue by *HSP31* overexpression could not be assessed in synthetic media for strains with the *atg8*Δ genotype because *GAL*-αSyn expression was not toxic in these strains (*middle*). Rescue of *GAL*-αSyn expression in the *hsp31*Δ strain was toxic and rescued by *HSP31* overexpression in synthetic and YEP media.

CS aggregation is triggered by elevated temperature, and we demonstrated that Hsp31 suppresses CS aggregation 6-fold more efficiently then hchA and DJ-1. Hsp31 also suppresses insulin aggregation, demonstrating that Hsp31 can maintain chaperone activity in a reducing environment in contrast to the redox-dependent DJ-1, which does not have activity in this assay.

Hsp31 also exhibited considerable activity in an *in vitro* αSyn fibrillization assay and completely suppressed fibrillization at a molar ratio of 8.75:1 (αSyn/Hsp31) and maintained considerable activity at a ratio of 35:1. DJ-1 also had activity at substoichiometric levels but required higher molar ratios compared with Hsp31. We consistently observed that the Hsp31-MORF purified from yeast was more active than recombinant Hsp31, DJ-1, or hchA (Fig. 1, *B* and *D*). This could be due to the fusion tag type or fusion orientation affecting protein activity, which has been noted previously for hchA (17, 18). Further studies are needed to delineate the source of these activity differences, including the possibility that it is related to the purification procedure, oxidation state of the protein, oligomeric state, or post-translational modifications. The broad range of substrates and substoichiometric activity all indicate that Hsp31 is a chaperone with robust activity compared with other members of this superfamily.

Despite the fact that its cellular function is incompletely understood, αSyn is known to aggregate and form inclusions. These protein inclusions are precursors of Lewy bodies, the pathological hallmark of PD. Elucidating mechanisms of αSyn aggregation is important to understand PD pathogenesis, and the heterologous expression of αSyn in yeast established a useful platform to investigate αSyn biology (9). We extended the αSyn yeast model by demonstrating the modulation of αSyn toxicity and subcellular localization by Hsp31. Expression of 2x*GAL*-αSyn is toxic to yeast cells, and constitutive expression of Hsp31 from the *GPD* promoter rescued cells from αSyn-mediated toxicity (Fig. 2). In addition, expression of one copy of *GAL*-αSyn is not toxic to wild-type cells but is toxic in the *hsp31*Δ strain. Taken together, it appears that the chaperone effect of Hsp31 is necessary to maintain cellular fitness upon αSyn expression.

Hsp31 also altered the subcellular localization profile of αSyn. Expression of 2x*GAL*-αSyn results in cytosolic accumulations (foci), whereas the expression of one copy of *GAL*-αSyn results in primarily plasma membrane localization. The *in vivo*

cytoplasmic foci are associated with vesicular membranes (39), and analysis of cellular lysates indicates the presence of higher order oligomeric forms of αSyn, although the nature of this aggregation is unclear (23, 67). Expression of *GAL-HSP31* results in more than 2-fold suppression of foci and increases the localization of αSyn to the plasma membrane (Fig. 3*A*). This effect was transiently observed at 8 h postinduction, but a high rate of puncta formation returned after 24 h, possibly because Hsp31 expression was induced at the same time as αSyn. This is consistent with the result where *GAL-HSP31* does not rescue the synthetic lethal effect of αSyn expression in the *hsp31*Δ strain, whereas the constitutive *GPD-HSP31* rescues *hsp31*Δ. These results indicate that a higher threshold level of Hsp31 is needed in the cell prior to αSyn induction to prevent toxicity. The exact temporal relationship between Hsp31 expression and αSyn foci suppression could provide insight into the aggregation state of αSyn species targeted by Hsp31.

Several orthologous experiments suggest that Hsp31 interacts early in the misfolding process and prevents the formation of larger oligomeric species. The addition of Hsp31 to αSyn monomers in a fibrillization assay resulted in a baseline level of ThioT fluorescence signal, indicating that the formation of larger oligomeric species was prevented (Fig. 1*D*). Analysis of the SDS-resistant oligomeric species by SDS-PAGE demonstrated that the presence of Hsp31 prevented the formation of higher order oligomeric αSyn species (Fig. 7*A*). Our prion aggregation studies indicate that Hsp31 inhibits prion assembly before the formation of subcellular visible GFP-tagged PrD aggregates and those detected by SDD-AGE (Fig. 9*B*). Furthermore, the Sup35 aggregates occlude Hsp31, indicating that the anti-aggregation activity of Hsp31 commences prior to the formation of the visible aggregate and probably does not act to remove or disassemble any preformed aggregate (Fig. 9*A*). This is in contrast to large chaperones, Hsp104, Ssa1/2, Sis1, and Sse1, which mutually colocalize with prion aggregates (68). A previous study has demonstrated that small HSPs can inhibit the formation of Sup35 aggregates and found that Hsp26 and Hsp42 inhibit rare transient oligomers at distinctly different steps in the prion formation process (69). Further studies will be required to determine whether Hsp31 inhibits protein misfolding with a similar or distinct mechanism as Hsp26 or Hsp42. Overall, we demonstrate that Hsp31 can inhibit oligomerization or aggregation of many different proteins by intervening early in the process.

The role of Hsp31 in protecting cells from αSyn-mediated toxicity led us to investigate the expression of Hsp31 in response to proteotoxic stress and other types of stress. The expression pattern of Hsp31 in a genomically tagged strain decreased during log phase growth and increased at the diauxic shift and at saturation (Fig. 4). The increased expression of Hsp31 at the diauxic shift and in stationary phase could possibly be due to the stress of decreased nutrients or accumulation of metabolites associated with these growth phases and is part of a global transcriptional response program (70). An increase in Hsp31 expression in response to ROS has been observed previously (71), and we confirmed that our tagged strain behaved in a similar manner by demonstrating an increase in expression upon exposure to H_2O_2 (Fig. 4*B*). This ROS response has been implicated to be dependent on the Yap1 stress response transcription factor, and a shortened Hsp31 promoter (−313 bp relative to the ATG), which removes the Yap1 binding site (−363 and −353 bp relative to the ATG), has decreased Hsp31 expression in response to oxidative stress (72). However, we note that the shortened promoter also removes an additional stress response element (a CCCCT site at −379 to −383 from the ATG) in proximity to the Yap1 binding site. Stress response elements have been demonstrated to be the binding site for Msn2/4, and numerous stress-related yeast genes have been documented to be transcriptionally activated by these transcription factors (26), including genes up-regulated after the diauxic shift in stationary phase cells (26). Hsp31 appears to be part of the global transcriptional stress response by Yap1 and Msn2/4 or other stress-related transcription factors, such as Hsf1 or Gis1.

Finally, we also examined the response of Hsp31 expression during αSyn-initiated proteotoxic stress and observed an increased expression in cells in log phase. We measured an increase in superoxide levels upon αSyn expression consistent with a previous report that indicated that αSyn expression is associated with caspase-mediated ROS generation (73) (Fig. 3*D*). Deletion of *HSP31* also leads to increased superoxide levels with or without αSyn expression. These results establish that Hsp31 has a role in response to ROS, and its expression is induced in response to several types of stress.

We demonstrated the robust chaperone activity of Hsp31, but the *in vivo* rescue effects could have been mediated by the Hsp31 methylglyoxalase activity or interaction with other biological pathways, such as the metabolic or autophagy pathway. We confirmed that Hsp31 does have methylglyoxalase activity and demonstrated that mutation of the catalytic triad residue, C138D, results in greatly reduced methylglyoxalase activity (Fig. 5, *A* and *B*). However, this mutation did not inactivate the chaperone activity in the αSyn fibrillization assay (Fig. 7*C*), and expression of GPD-HSP31 C138D rescued cells from αSyn-mediated toxicity (Fig. 5*C*). Furthermore, we showed that that exogenous MGO did not differentially affect viability, suggesting that Hsp31 does not rescue by reducing accumulation of this toxic metabolite in αSyn-expressing cells (Fig. 6).

We also demonstrated that the autophagy pathway is an important mediator in the αSyn toxicity because deletion of *ATG8* resulted in synthetic lethal interaction with αSyn expression (Fig. 10*A*). This is consistent with *atg1*Δ or *atg7*Δ strains having synthetic lethal interactions with αSyn expression and having defects in clearing αSyn foci (74). However, we show that the *hsp31*Δ *atg8*Δ strain does not have increased αSyn-mediated toxicity when compared with *atg8*Δ, consistent with these genes occurring within the same synthetic lethal pathway. A recent result indicates that *hsp31*Δ strains are defective in autophagy (51), so the addition deletion of an autophagy gene should not increase toxicity. Interestingly, overexpression of Hsp31 in these autophagy-deficient strains can rescue cells from αSyn toxicity, indicating that the autophagy pathway is not essential for chaperone rescue (Fig. 10*B*). Autophagy may be beneficial for controlling αSyn toxicity, but it appears that chaperone activity of Hsp31 is also important. These experiments also are the first to delineate that enzymatic methylg-

lyoxalase activity of Hsp31 is not essential to rescue αSyn toxicity.

Our results suggest that Hsp31 functions as a cytoplasmic chaperone against a variety of misfolded proteins. Recent studies have demonstrated the facility of yeast to investigate pathogenic mechanisms underlying αSyn toxicity, including the identification of novel biological pathways that impinge on αSyn biology and small molecule modulators of αSyn toxicity (66, 69). In addition, the action of Hsp31 on αSyn may provide insight into the mode of toxicity of αSyn because recent evidence suggests that the αSyn toxic species is smaller than the visible aggregate (66). It should be noted that the prion expression studies done in this study were not completed with [*PSI*+] strains, but further studies using such strains would be of interest to determine the effect of Hsp31 on prion initiation and propagation.

We have established a framework that extends the yeast model for investigating mechanisms of αSyn toxicity in the context of the DJ-1/ThiJ/PfpI superfamily in yeast. Extension of this work will assist in elucidation of the chaperone-like mechanisms of Hsp31, and a comparison with DJ-1 may provide evolutionary insights into the activities of the DJ-1/PfpI/ThiJ superfamily. Our model may also be used to further delineate the nature of oligomeric species in the pathogenesis of PD and possibly what species of αSyn should be targeted therapeutically.

Author Contributions—C. T., K. A., J-C. R., and T. H. wrote the paper. J-C. R. and T. H. conceived and coordinated the study. C. T. constructed plasmids, strains, and purified proteins for this study. C. T. performed experiments and analyzed experiments in Figs. 1, 2, 3, 4, and 7. K. A. performed and analyzed experiments in Figs. 5, 6, 8, 9, and 10. H. M. D. performed and analyzed the citrate synthase studies, K. M. G. ascertained the Hsp31 expression with oxidative stress, and J. M. A. provided technical assistance and analysis of αSyn protein purification and assessment. L. N. P. provided technical assistance and contributed to sedimentation ultracentrifugation studies. All authors reviewed the results and approved the final version of the manuscript.

Acknowledgments—We thank Dr. Susan Lindquist (MIT) and Dr. François Baneyx (University of Washington) for strains and plasmids. Confocal imaging was assisted by Dr. Li Li (Purdue Live Cell Imaging Facility).

References

1. Luo, G. R., Chen, S., and Le, W. D. (2007) Are heat shock proteins therapeutic target for Parkinson's disease? *Int. J. Biol. Sci.* **3,** 20–26
2. Vila, M., and Przedborski, S. (2004) Genetic clues to the pathogenesis of Parkinson's disease. *Nat. Med.* **10,** S58–S62
3. Farrer, M. J. (2006) Genetics of Parkinson disease: paradigm shifts and future prospects. *Nat. Rev. Genet.* **7,** 306–318
4. Batelli, S., Albini, D., Rametta, R., Polito, L., Prato, F., Pesaresi, M., Negro, A., Forloni, G. (2008) DJ-1 modulates α-synuclein aggregation state in a cellular model of oxidative stress: relevance for Parkinson's disease and involvement of HSP70. *PLoS One* **3,** e1884
5. Choi, J., Sullards, M. C., Olzmann, J. A., Rees, H. D., Weintraub, S. T., Bostwick, D. E., Gearing, M., Levey, A. I., Chin, L.-S., and Li, L. (2006) Oxidative damage of DJ-1 is linked to sporadic Parkinson's and Alzheimer's diseases. *J. Biol. Chem.* **281,** 10816–10824
6. Esteves, A. R., Arduíno, D. M., Swerdlow, R. H., Oliveira, C. R., and Cardoso, S. M. (2009) Oxidative stress involvement in α-synuclein oligomerization in Parkinson's disease cybrids. *Antioxid. Redox. Signal.* **11,** 439–448
7. Hsu, L. J., Sagara, Y., Arroyo, A., Rockenstein, E., Sisk, A., Mallory, M., Wong, J., Takenouchi, T., Hashimoto, M., and Masliah, E. (2000) α-Synuclein promotes mitochondrial deficit and oxidative stress. *Am. J. Pathol.* **157,** 401–410
8. Jellinger, K. A. (2010) Basic mechanisms of neurodegeneration: a critical update. *J. Cell Mol. Med.* **14,** 457–487
9. Shendelman, S., Jonason, A., Martinat, C., Leete, T., and Abeliovich, A. (2004) DJ-1 is a redox-dependent molecular chaperone that inhibits α-synuclein aggregate formation. *PLoS Biol.* **2,** e362
10. Lucas, J. I., and Marín, I. (2007) A new evolutionary paradigm for the Parkinson disease gene DJ-1. *Mol. Biol. Evol.* **24,** 551–561
11. Kahle, P. J., Waak, J., and Gasser, T. (2009) DJ-1 and prevention of oxidative stress in Parkinson's disease and other age-related disorders. *Free Radic. Biol. Med.* **47,** 1354–1361
12. Lev, N., Roncevic, D., Ickowicz, D., Melamed, E., and Offen, D. (2006) Role of DJ-1 in Parkinson's disease. *J. Mol. Neurosci.* **29,** 215–225
13. Taira, T., Saito, Y., Niki, T., Iguchi-Ariga, S. M. M., Takahashi, K., and Ariga, H. (2004) DJ-1 has a role in antioxidative stress to prevent cell death. *EMBO Rep.* **5,** 213–218
14. Liu, F., Nguyen, J. L., Hulleman, J. D., Li, L., and Rochet, J. C. (2008) Mechanisms of DJ-1 neuroprotection in a cellular model of Parkinson's disease. *J. Neurochem.* **105,** 2435–2453
15. Bandyopadhyay, S., and Cookson, M. (2004) Evolutionary and functional relationships within the DJ1 superfamily. *BMC Evol. Biol.* **4,** 6
16. Lee, S. J., Kim, S. J., Kim, I. K., Ko, J., Jeong, C. S., Kim, G. H., Park, C., Kang, S. O., Suh, P. G., Lee, H. S., and Cha, S. S. (2003) Crystal structures of human DJ-1 and *Escherichia coli* Hsp31, which share an evolutionarily conserved domain. *J. Biol. Chem.* **278,** 44552–44559
17. Wilson, M. A., St Amour, C. V., Collins, J. L., Ringe, D., and Petsko, G. A. (2004) The 1.8-Å resolution crystal structure of YDR533Cp from *Saccharomyces cerevisiae*: a member of the DJ-1/ThiJ/PfpI superfamily. *Proc. Natl. Acad. Sci. U.S.A.* **101,** 1531–1536
18. Graille, M., Quevillon-Cheruel, S., Leulliot, N., Zhou, C. Z., Li de la Sierra Gallay, I., Jacquamet, L., Ferrer, J. L., Liger, D., Poupon, A., Janin, J., and van Tilbeurgh, H. (2004) Crystal structure of the YDR533c *S. cerevisiae* protein, a class II member of the Hsp31 family. *Structure* **12,** 839–847
19. Wei, Y., Ringe, D., Wilson, M. A., and Ondrechen, M. J. (2007) Identification of functional subclasses in the DJ-1 superfamily proteins. *PLoS Comput. Biol.* **3,** e10
20. Wilson, M. A. (2014) Metabolic role for yeast DJ-1 superfamily proteins. *Proc. Natl. Acad. Sci. U.S.A.* **111,** 6858–6859
21. Zondler, L., Miller-Fleming, L., Repici, M., Gonçalves, S., Tenreiro, S., Rosado-Ramos, R., Betzer, C., Straatman, K. R., Jensen, P. H., Giorgini, F., and Outeiro, T. F. (2014) DJ-1 interactions with α-synuclein attenuate aggregation and cellular toxicity in models of Parkinson's disease. *Cell Death Dis.* **5,** e1350
22. Miller-Fleming, L., Antas, P., Pais, T. F., Smalley, J. L., Giorgini, F., and Outeiro, T. F. (2014) Yeast DJ-1 superfamily members are required for diauxic-shift reprogramming and cell survival in stationary phase. *Proc. Natl. Acad. Sci. U.S.A.* **111,** 7012–7017
23. Outeiro, T. F., and Lindquist, S. (2003) Yeast cells provide insight into α-synuclein biology and pathobiology. *Science* **302,** 1772–1775
24. Willingham, S., Outeiro, T. F., DeVit, M. J., Lindquist, S. L., and Muchowski, P. J. (2003) Yeast genes that enhance the toxicity of a mutant huntingtin fragment or α-synuclein. *Science* **302,** 1769–1772
25. Cooper, A. A., Gitler, A. D., Cashikar, A., Haynes, C. M., Hill, K. J., Bhullar, B., Liu, K., Xu, K., Strathearn, K. E., Liu, F., Cao, S., Caldwell, K. A., Caldwell, G. A., Marsischky, G., Kolodner, R. D., Labaer, J., Rochet, J. C., Bonini, N. M., and Lindquist, S. (2006) α-Synuclein blocks ER-Golgi traffic and Rab1 rescues neuron loss in Parkinson's models. *Science* **313,** 324–328
26. Skoneczna, A., Miciałkiewicz, A., and Skoneczny, M. (2007) *Saccharomyces cerevisiae* Hsp31p, a stress response protein conferring protection against reactive oxygen species. *Free Radic. Biol. Med.* **42,** 1409–1420

27. Kim, I. S., Sohn, H. Y., and Jin, I. (2011) Adaptive stress response to menadione-induced oxidative stress in *Saccharomyces cerevisiae* KNU5377. *J. Microbiol.* **49,** 816–823
28. Takanishi, C. L., and Wood, M. J. (2011) A genetically encoded probe for the identification of proteins that form sulfenic acid in response to H_2O_2 in *Saccharomyces cerevisiae*. *J. Proteome Res.* **10,** 2715–2724
29. de Melo, H. F., Bonini, B. M., Thevelein, J., Simões, D. A., and Morais, M. A., Jr. (2010) Physiological and molecular analysis of the stress response of *Saccharomyces cerevisiae* imposed by strong inorganic acid with implication to industrial fermentations. *J. Appl. Microbiol.* **109,** 116–127
30. Amberg, D., Burke, D., and Strathern, J. (2005) *Methods in Yeast Genetics: A Cold Spring Harbor Laboratory Course Manual*, 2005 Ed., Cold Spring Harbor Laboratory Press, Cold Spring Harbor, NY
31. Janke, C., Magiera, M. M., Rathfelder, N., Taxis, C., Reber, S., Maekawa, H., Moreno-Borchart, A., Doenges, G., Schwob, E., Schiebel, E., and Knop, M. (2004) A versatile toolbox for PCR-based tagging of yeast genes: new fluorescent proteins, more markers and promoter substitution cassettes. *Yeast* **21,** 947–962
32. Alberti, S., Gitler, A. D., and Lindquist, S. (2007) A suite of Gateway® cloning vectors for high-throughput genetic analysis in *Saccharomyces cerevisiae*. *Yeast* **24,** 913–919
33. Gelperin, D. M., White, M. A., Wilkinson, M. L., Kon, Y., Kung, L. A., Wise, K. J., Lopez-Hoyo, N., Jiang, L., Piccirillo, S., Yu, H., Gerstein, M., Dumont, M. E., Phizicky, E. M., Snyder, M., and Grayhack, E. J. (2005) Biochemical and genetic analysis of the yeast proteome with a movable ORF collection. *Genes Dev.* **19,** 2816–2826
34. Conway, K. A., Harper, J. D., and Lansbury, P. T., Jr. (2000) Fibrils formed in vitro from α-synuclein and two mutant forms linked to Parkinson's disease are typical amyloid. *Biochemistry* **39,** 2552–2563
35. Rochet, J. C., Conway, K. A., and Lansbury, P. T., Jr. (2000) Inhibition of fibrillization and accumulation of prefibrillar oligomers in mixtures of human and mouse α-synuclein. *Biochemistry* **39,** 10619–10626
36. Krasnoslobodtsev, A. V., Peng, J., Asiago, J. M., Hindupur, J., Rochet, J. C., and Lyubchenko, Y. L. (2012) Effect of spermidine on misfolding and interactions of α-synuclein. *PLoS One* **7,** e38099
37. Brown, P. H., and Schuck, P. (2006) Macromolecular size-and-shape distributions by sedimentation velocity analytical ultracentrifugation. *Biophys. J.* **90,** 4651–4661
38. Sastry, M. S., Korotkov, K., Brodsky, Y., and Baneyx, F. (2002) Hsp31, the *Escherichia coli yedU* gene product, is a molecular chaperone whose activity is inhibited by ATP at high temperatures. *J. Biol. Chem.* **277,** 46026–46034
39. Sastry, M. S., Zhou, W., and Baneyx, F. (2009) Integrity of N- and C-termini is important for *E. coli* Hsp31 chaperone activity. *Protein Sci.* **18,** 1439–1447
40. Hoyer, W., Antony, T., Cherny, D., Heim, G., Jovin, T. M., and Subramaniam, V. (2002) Dependence of α-synuclein aggregate morphology on solution conditions. *J. Mol. Biol.* **322,** 383–393
41. Wenig, P., and Odermatt, J. (2010) OpenChrom: a cross-platform open source software for the mass spectrometric analysis of chromatographic data. *BMC Bioinformatics* **11,** 405
42. Halfmann, R., and Lindquist, S. (2008) Screening for amyloid aggregation by semi-denaturing detergent-agarose gel electrophoresis. *J. Vis. Exp.* **17,** e838
43. Malki, A., Kern, R., Abdallah, J., and Richarme, G. (2003) Characterization of the *Escherichia coli* YedU protein as a molecular chaperone. *Biochem. Biophys. Res. Commun.* **301,** 430–436
44. Marini, I., Moschini, R., Del Corso, A., and Mura, U. (2005) Chaperone-like features of bovine serum albumin: a comparison with α-crystallin. *Cell Mol. Life Sci.* **62,** 3092–3099
45. Choi, D., Ryu, K. S., and Park, C. (2013) Structural alteration of *Escherichia coli* Hsp31 by thermal unfolding increases chaperone activity. *Biochim. Biophys. Acta* **1834,** 621–628
46. Zhou, W., Zhu, M., Wilson, M. A., Petsko, G. A., and Fink, A. L. (2006) The oxidation state of DJ-1 regulates its chaperone activity toward α-synuclein. *J. Mol. Biol.* **356,** 1036–1048
47. Zhou, W., and Freed, C. R. (2005) DJ-1 up-regulates glutathione synthesis during oxidative stress and inhibits A53T α-synuclein toxicity. *J. Biol. Chem.* **280,** 43150–43158
48. Kirik, D., Rosenblad, C., Burger, C., Lundberg, C., Johansen, T. E., Muzyczka, N., Mandel, R. J., and Björklund, A. (2002) Parkinson-like neurodegeneration induced by targeted overexpression of α-synuclein in the nigrostriatal system. *J. Neurosci.* **22,** 2780–2791
49. Ko, L. W., Ko, H. H., Lin, W. L., Kulathingal, J. G., and Yen, S. H. (2008) Aggregates assembled from overexpression of wild-type α-synuclein are not toxic to human neuronal cells. *J. Neuropathol. Exp. Neurol.* **67,** 1084–1096
50. Lee, H. J., and Lee, S. J. (2002) Characterization of cytoplasmic α-synuclein aggregates: fibril formation is tightly linked to the inclusion-forming process in cells. *J. Biol. Chem.* **277,** 48976–48983
51. Flower, T. R., Chesnokova, L. S., Froelich, C. A., Dixon, C., and Witt, S. N. (2005) Heat shock prevents α-synuclein-induced apoptosis in a yeast model of Parkinson's disease. *J. Mol. Biol.* **351,** 1081–1100
52. Miura, T., Minegishi, H., Usami, R., and Abe, F. (2006) Systematic analysis of HSP gene expression and effects on cell growth and survival at high hydrostatic pressure in *Saccharomyces cerevisiae*. *Extremophiles* **10,** 279–284
53. Hasim, S., Hussin, N. A., Alomar, F., Bidasee, K. R., Nickerson, K. W., and Wilson, M. A. (2014) A glutathione-independent glyoxalase of the DJ-1 superfamily plays an important role in managing metabolically generated methylglyoxal in *Candida albicans*. *J. Biol. Chem.* **289,** 1662–1674
54. Zhao, Q., Su, Y., Wang, Z., Chen, C., Wu, T., and Huang, Y. (2014) Identification of glutathione (GSH)-independent glyoxalase III from *Schizosaccharomyces pombe*. *BMC Evol. Biol.* **14,** 86
55. Lee, J. Y., Song, J., Kwon, K., Jang, S., Kim, C., Baek, K., Kim, J., and Park, C. (2012) Human DJ-1 and its homologs are novel glyoxalases. *Hum. Mol. Genet.* **21,** 3215–3225
56. Angeloni, C., Zambonin, L., and Hrelia, S. (2014) Role of methylglyoxal in Alzheimer's disease. *Biomed. Res. Int.* **2014,** 238485
57. Vistoli, G., De Maddis, D., Cipak, A., Zarkovic, N., Carini, M., and Aldini, G. (2013) Advanced glycoxidation and lipoxidation end products (AGEs and ALEs): an overview of their mechanisms of formation. *Free. Radic. Res.* **47,** 3–27
58. Shaikh, S., and Nicholson, L. F. (2008) Advanced glycation end products induce *in vitro* cross-linking of α-synuclein and accelerate the process of intracellular inclusion body formation. *J. Neurosci. Res.* **86,** 2071–2082
59. Bito, A., Haider, M., Hadler, I., and Breitenbach, M. (1997) Identification and phenotypic analysis of two glyoxalase II encoding genes from *Saccharomyces cerevisiae*, *GLO2* and *GLO4*, and intracellular localization of the corresponding proteins. *J. Biol. Chem.* **272,** 21509–21519
60. Inoue, Y., and Kimura, A. (1996) Identification of the structural gene for glyoxalase I from *Saccharomyces cerevisiae*. *J. Biol. Chem.* **271,** 25958–25965
61. Kvam, E., Nannenga, B. L., Wang, M. S., Jia, Z., Sierks, M. R., and Messer, A. (2009) Conformational targeting of fibrillar polyglutamine proteins in live cells escalates aggregation and cytotoxicity. *PLoS One* **4,** e5727
62. Nixon, R. A. (2013) The role of autophagy in neurodegenerative disease. *Nat. Med.* **19,** 983–997
63. Qi, L., and Zhang, X. D. (2014) Role of chaperone-mediated autophagy in degrading Huntington's disease-associated huntingtin protein. *Acta Biochim. Biophys. Sin.* **46,** 83–91
64. Au, A. K., Bayir, H., Kochanek, P. M., and Clark, R. S. (2010) Evaluation of autophagy using mouse models of brain injury. *Biochim. Biophys. Acta* **1802,** 918–923
65. Juhász, G., Erdi, B., Sass, M., and Neufeld, T. P. (2007) Atg7-dependent autophagy promotes neuronal health, stress tolerance, and longevity but is dispensable for metamorphosis in *Drosophila*. *Genes Dev.* **21,** 3061–3066
66. Petroi, D., Popova, B., Taheri-Talesh, N., Irniger, S., Shahpasandzadeh, H., Zweckstetter, M., Outeiro, T. F., and Braus, G. H. (2012) Aggregate clearance of α-synuclein in *Saccharomyces cerevisiae* depends more on autophagosome and vacuole function than on the proteasome. *J. Biol. Chem.* **287,** 27567–27579
67. Miller-Fleming, L., Giorgini, F., and Outeiro, T. F. (2008) Yeast as a model for studying human neurodegenerative disorders. *Biotechnol. J.* **3,** 325–338
68. Gitler, A. D., Bevis, B. J., Shorter, J., Strathearn, K. E., Hamamichi, S., Su,

L. J., Caldwell, K. A., Caldwell, G. A., Rochet, J. C., McCaffery, J. M., Barlowe, C., and Lindquist, S. (2008) The Parkinson's disease protein α-synuclein disrupts cellular Rab homeostasis. *Proc. Natl. Acad. Sci. U.S.A.* **105,** 145–150

69. Tenreiro, S., Reimão-Pinto, M. M., Antas, P., Rino, J., Wawrzycka, D., Macedo, D., Rosado-Ramos, R., Amen, T., Waiss, M., Magalhães, F., Gomes, A., Santos, C. N., Kaganovich, D., and Outeiro, T. F. (2014) Phosphorylation modulates clearance of α-synuclein inclusions in a yeast model of Parkinson's disease. *PLoS Genet.* **10,** e1004302
70. Saibil, H. R., Seybert, A., Habermann, A., Winkler, J., Eltsov, M., Perkovic, M., Castaño-Diez, D., Scheffer, M. P., Haselmann, U., Chlanda, P., Lindquist, S., Tyedmers, J., and Frangakis, A. S. (2012) Heritable yeast prions have a highly organized three-dimensional architecture with interfiber structures. *Proc. Natl. Acad. Sci. U.S.A.* **109,** 14906–14911
71. Duennwald, M. L., Echeverria, A., and Shorter, J. (2012) Small heat shock proteins potentiate amyloid dissolution by protein disaggregases from yeast and humans. *PLos Biol.* **10,** e1001346
72. Galdieri, L., Mehrotra, S., Yu, S., and Vancura, A. (2010) Transcriptional regulation in yeast during diauxic shift and stationary phase. *OMICS* **14,** 629–638
73. Morano, K. A., Grant, C. M., and Moye-Rowley, W. S. (2012) The response to heat shock and oxidative stress in *Saccharomyces cerevisiae*. *Genetics* **190,** 1157–1195
74. Trott, A., and Morano, K. A. (2003) in *Yeast Stress Responses* (Hohman, S., and Mager, W. H., eds) pp. 71–119, Springer, Berlin
75. Tardiff, D. F., Jui, N. T., Khurana, V., Tambe, M. A., Thompson, M. L., Chung, C. Y., Kamadurai, H. B., Kim, H. T., Lancaster, A. K., Caldwell, K. A., Caldwell, G. A., Rochet, J. C., Buchwald, S. L., and Lindquist, S. (2013) Yeast reveal a "druggable" Rsp5/Nedd4 network that ameliorates α-synuclein toxicity in neurons. *Science* **342,** 979–983
76. Chung, C. Y., Khurana, V., Auluck, P. K., Tardiff, D. F., Mazzulli, J. R., Soldner, F., Baru, V., Lou, Y., Freyzon, Y., Cho, S., Mungenast, A. E., Muffat, J., Mitalipova, M., Pluth, M. D., Jui, N. T., Schüle, B., Lippard, S. J., Tsai, L. H., Krainc, D., Buchwald, S. L., Jaenisch, R., and Lindquist, S. (2013) Identification and rescue of α-synuclein toxicity in Parkinson patient-derived neurons. *Science* **342,** 983–987
77. Sharma, N., Brandis, K. A., Herrera, S. K., Johnson, B. E., Vaidya, T., Shrestha, R., and Debburman, S. K. (2006) α-Synuclein budding yeast model: toxicity enhanced by impaired proteasome and oxidative stress. *J. Mol. Neurosci.* **28,** 161–178
78. Su, L. J., Auluck, P. K., Outeiro, T. F., Yeger-Lotem, E., Kritzer, J. A., Tardiff, D. F., Strathearn, K. E., Liu, F., Cao, S., Hamamichi, S., Hill, K. J., Caldwell, K. A., Bell, G. W., Fraenkel, E., Cooper, A. A., Caldwell, G. A., McCaffery, J. M., Rochet, J. C., and Lindquist, S. (2010) Compounds from an unbiased chemical screen reverse both ER-to-Golgi trafficking defects and mitochondrial dysfunction in Parkinson's disease models. *Dis. Model. Mech.* **3,** 194–208
79. Paleologou, K. E., Schmid, A. W., Rospigliosi, C. C., Kim, H. Y., Lamberto, G. R., Fredenburg, R. A., Lansbury, P. T., Jr., Fernandez, C. O., Eliezer, D., Zweckstetter, M., and Lashuel, H. A. (2008) Phosphorylation at Ser-129 but not the phosphomimics S129E/D inhibits the fibrillation of α-synuclein. *J. Biol. Chem.* **283,** 16895–16905